LA PRIMAVERA GEOTHERMAL DEVELOPMENT PROJECT

IN UNITED MEXICAN STATES

INTERIM REPORT

SEPTEMBER, 1986

JAPAN INTERNATIONAL COOPERATION AGENCY

RESUMEN

Las fracturas existentes hasta una profundidad de aproximadamente 1000 m consisten principalmente en el sistema de fallas normales de rumbo NE - SW, en con - cordancia con la orientación estructural NE - SW en - contrada por los estudios de alteración hidrotermal de las rocas, concentración de mercurio en el suelo, y prospección gravimétrica. Por el contrario, el modelo de fracturación a profundidades superiores a 1000 m se cree formado por fracturas extensionales de alto ángu - lo, con dirección NW - SE, conforme al análisis es - tructural de las rocas del basamento y de series ter - ciarias, y a la orientación de la zona de baja resis - tividad revelada por la prospección eléctrica mediante el metodo magnetotelúrico.

A juzgar por los resultados de las medidas de tem - peratura en el interior de sondeos, temperatura mínima de homogeneización de las inclusiones fluidas y com - posición química del fluido de sondeos, en las proxi - midades de PR-1 y PR-8 existe una zona de flujo ascen - dente de alta temperatura.

El campo geotérmico de Sierra La Primavera se carac - teriza por un yacimiento vertical, cuya parte elevada coincide prácticamente con la zona de flujo ascendente.

En la elección de objetivos geológicos para la perforación de sondeos de exploración destinados a evaluar el yacimiento geotérmico, C. F. E. tiende a poner énfasis exclusivamente en la geología de superficie. Sin embargo, el comportamiento de las fracturas varía fácilmente en profundidad a altas temperaturas y presiones, así como en yacimientos sometidos a movimientos tectónicos distintos de los detectables mediante geología de superficie.

En el caso de un yacimiento vertical, tanto la temperatura como el grado de fracturación disminuyen con la distancia a la zona de flujo ascendente. Por lo tanto, es indispensable perforar a través del sistema de fracturación profundo, que se estima orientado en dirección NW - SE.

En la primera fase de la exploración se proponía la perforación de 3 pozos térmicos de 750 m de profundidad durante el año fiscal 1986. Sin embargo, dado que de los estudios llevados a cabo en el año fiscal 1985 se ha obtenido suficiente información sobre la extensión del yacimiento geotérmico y la distribución de temperatura en el subsuelo, es preferible modificar el plan de trabajo en el año fiscal 1986 de la siguiente manera : perforación de un sondeo de exploración de aproximadamente 2000 m en lugar de los tres pozos térmicos.

INTRODUCTION

The full-scale survey by JICA study team has been carried out during the period from June 1985 to February 1986 on the site in Sierra La Primavera Geothermal Area in United Mexican States. From the results of data analysis of surveys, it has become clear the structure and extent of the geothermal reservoir in this area. Moreover, the targets of drilling for exploration wells were selected on the basis of the results ultimately.

The survey results were made a report and discussed with C.F.E. from the 21th of July to the 3rd of August in 1986, including selection of target point on the site.

This report describes the full-scale survey implemented in detail and evaluates the structure and extent of the reservoir by means of a comprehensive analysis. In addition, it refers to the proposal for the work plan of next stage and also the targets of drilling for exploration wells.

Essential support for these investigations comes from C.F.E. and associated people. We are sincerely grateful to them for all cooperations.

CONTENTS

List of illustrations

I. General Remarks

I. GENERAL REMARKS

I-I. The purpose of survey

The purpose of survey on La Primavera geothermal development project is to evaluate the geothermal reservoir in this area and to determine the possible development output of planned power station by analyzing the data obtained from both the wells drilled by C.F.E. and the results done by JICA study team.

The survey includes the following items:

(1) Detailed geological survey including core and cutting analyses of the wells drilled by C.F.E.

(2) Geochemical analyses of mercury in soil and wellbore fluid

(3) Gravimetric survey

(4) Electrical survey (MT method)

(5) Well test under the condition of steam production

(6) Comprehensive analysis on geothermal reservoir

I-2. The term of survey on the site in FY 1985

(1) Geological survey by 4 geologists: from the 12th of June to the 9th of August.

(2) The first geochemical survey by 2 geochemists and gravimetric survey by 2 geophysicists : from the 24th of July to the 20th of September.

(3) Electrical survey by 3 geophysicists : from 27th of November to the 31th of January in 1986.

(4) The second geochemical survey by a geochemist : from 21th of January to the 14th of February.

(5) Well test by 2 reservoir engineers : from 21th of January to the 27th of February.

I-3. Summary of the results of survey

Locality map of the survey area is shown in Fig. 1. summary of the results of survey in 1985 is given as follows:

(1) Stratigraphy in the survey area

The basement rocks composed of granodiorite and quartzmonzonite are recognized in the depth from 2,840m to 2,986m of the bottom of PR-9 well. Basaltic andesite, rhyolite and rhyolitic tuff belonging to the Cordilleran Volcanics are underlain by the basement with about 2,500m in thickness, and overlain by the Tala Tuff which is pyroclastie flow extruded with the formation of Sierra La Primavera Caldera. Average thickness of Tala Tuff is about 500m. Tala Tuff is covered by the lake deposits distributed in the caldera lake formed by depression.

The rhyolites related to caldera domes are distributed in the lower and upper portion of the lake deposits in the northern half of this area.

(2) Distribution of fractures

The geological structure near the surface is characterized by normal faults with NE-SW direction. Distributions of hydrothermal rock alteration and also high concentration spots of mercury in soil coincide with the NE-SW faults.

Judging from the result of core analysis showing stress field was put under the same condition as that near the surface, it was understood that the upper Cordilleran Volcanics, namely to the depth of 1,000m from the surface, and cut by the fractures with NE-SW direction. As to the fracture system in the lower Cordilleran Volcanics which is regarded as the main geothermal

reservoir, the fractures with NW-SE direction are induced to be predominant on the basis of geological survey in the outside area of Caldera where the same formation is exposed at the ground outcrop. The fact that the fractures take NW-SE direction is supported by the result of electrical survey (MT method), showing that the deep seated low resistivity zone has NW-SE direction at south side of PR-8.

As conclusion, the fracture system is characterized by fractures with NW-SE direction at the deeper than 1,000m. The fractures are high angle extensional, because the influence of resurgent uplift after caldera forming is more significant in this place. The faults with NW-SE direction which is recognized at the surface have a different character, but it is not clear whether the faults connect with the deep seated fracture with NW-SE direction.

(3) Lost circulation points in the boreholes

Drill holes mainly encountered lost circulations during drilling of the Tala Tuff and the lower part of Cordilleran Volcanics. Lost circulations of the Tala Tuff indicate tensional fractures which have random directions and include that of thermal stress origin during cooling stage of pyroclastics. Lost circulations of the lower part of Cordilleran Volcanics are caused by encounter to the deeper seated fractures with NW-SE direction.

The fractures which yield excellent steam correspond to the complete losses of Cordilleran Volcanics at 1,800m level.

(4) Permeability of formations

Transmissibility around the wells can be calculated from the result of pressure measurement in the wells at different flowing state, showing $Kh=7.6\times10^{-13}\ m^3$ in PR-1 and $2.1\times10^{-13}\ m^3$ in PR-8. The values are smaller than 1 darcy·m (10^{-12} m^3), namely meaning not high permeability. Nevertheless, the both wells have high production of geothermal fluid. This is due to the reason that initial temperature is remarkably high.

(5) Distribution of subsurface temperature

The upflow zone of high temperature (about 300°C) is recognized near PR-1 and PR-8, judging from the results of downhole temperature measurements for wells and minimum homogenization temperature determination of fluid in cuttings. Geothermal fluid in this area is ascending from subsurface deeper portion through the channel near PR-1 and PR-8. The results of well test in PR-1 and PR-8 show that the flow condition in both wellbores is a flashed two-phase throughout the whole depth after flashing in the formation surrounding the wells.

(6) Chemistry and movement of geothermal fluid

In order to detect the movement of geothermal fluid in the underground, the relation between Cl^- concentration and enthalpy of deep hot water was checked. The relation shows that deep hot water existing near PR-1 is diluted by low Cl^- concentration and low enthalpy underground water in flowing from PR-1 to PR-8, PR-5 and PR-4.

Hot water of PR-2 is considered to be derived from another separated reservoir.

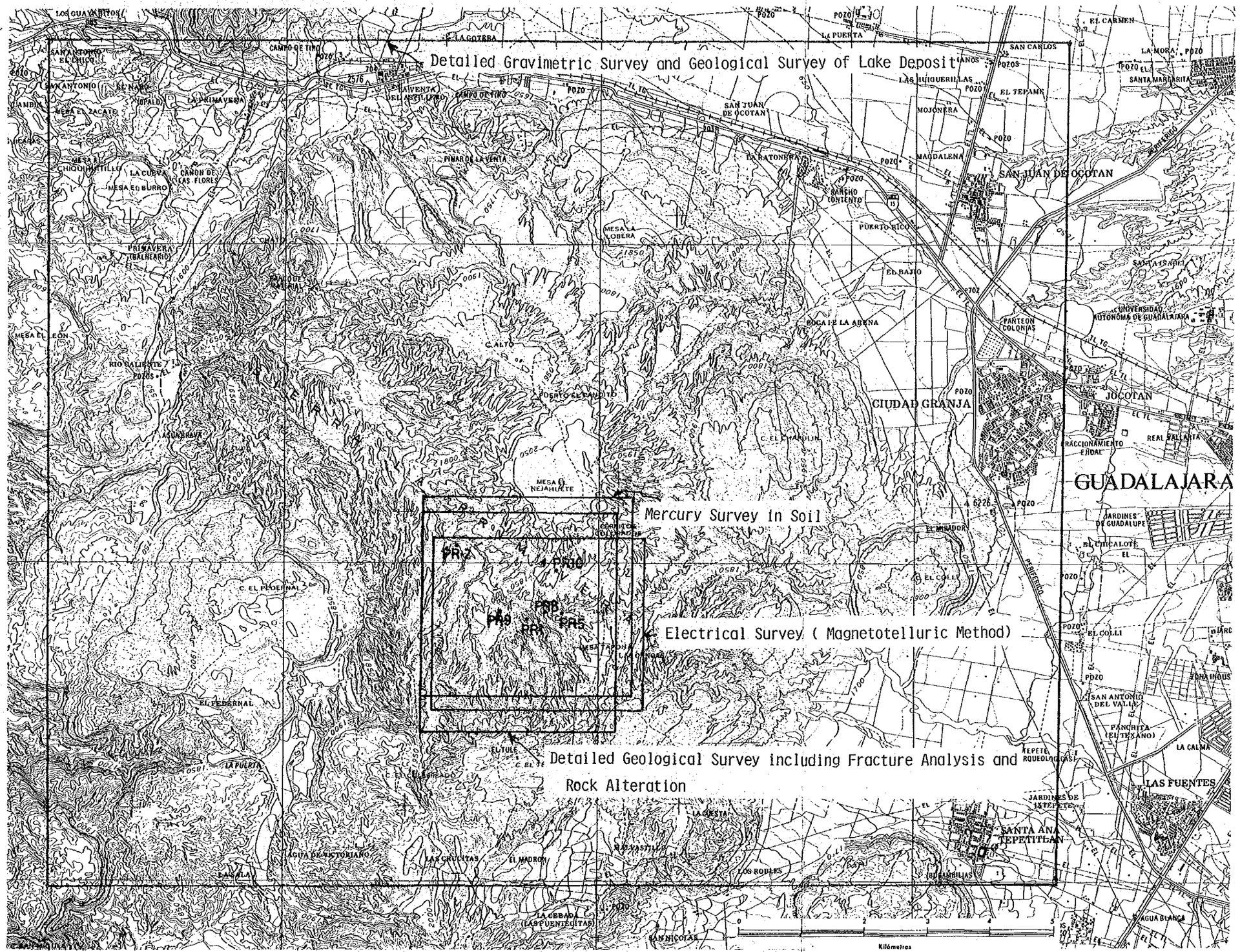

Fig. 1. Locality map of survey area

Ⅱ. Results of survey

II. RESULTS OF SURVEY

II-1 Geological survey

Geological survey includes two types of survey, namely field and core and cuttings surveys. Fracture analysis, rock alteration survey and sedimentary analysis of the lake deposits have been carried out in the field based on making of route map of 1:2,000 in scale. Moreover, geological survey of Tertiary System which is main reservoir in this area has been also done at the outside of Caldera to make clear the structure and rock facies of Tertiary System.

Measurements were made on the physical properties of rock cores including density, porosity and thermal conductivity and on the various characteristics of cutting such as magnetic susceptibility, chemical concentration of Hg and As, mineral identification by X-ray and fluid inclusion. Cores and cuttings were collected from the wells existed (PR-1,2,5,8 and RC-1).

(1) Geology in the geothermal manifestation area

Granodiorite and Quartz-Monzonite are observed in Well PR-9 (2,840 - 2,986m). They appear to be correlated in the granitic rocks of the Mesozoic to Neogene which are widely distributed on the Pacific Coast to the SE of the area. Volcanics of 2,500 m in Thickness are underlain by these "basement". The Volcanics belong to "Sierra Madre Occidental" consisting of basaltic andesite, rhyolite lava or rhyolitic tuff. Lithic tuff in PR-1 at ca 900m is very similar to the weakly welded pyroclastics of the Cordilleran Volcanics (CLOUGH, 1981) which is distributed in the north of Guadulajara City. Therefore, they probably belong to a

same formation. The Tala Tuff is pyroclastics originating from Sierra La Primavera Caldera Formation ca.95,000 years ago, and is pilded up with ca.500m thickness on the Cordilleran Volcanics (Fig. 2). The Tala Tuff could be divided into more than 11 flow units according to the present investigation and the well data. It is assumed that the collapse of Caldera did not occur at a single stroke and that the explosion and the collapse proceeded on simultaneously. The Tala Tuff contains a denser part in the middle and non-welded part in both upper and lower zones. Stratifications were observed in the non-welded parts containing surge-like sediments. Furthermore, Pumice Fall is found at the bottom.

In the northern half of this area, rhyolite lava is distributed under Lake deposites and above the Tala Tuff. The distribution of the leva is localized with thickness of 0 - 100m (thicker in the East). The Rhyolite is older than that of Older Ring Domes (MAHOOD, 1980) and assumed to be originated in the Lava Dome which came up at the collapse center. This is called the Cerritos Colorados Rhyolite in Fig. 2 and 3. Rhyolite is also located above the Lake deposites. It belongs to Older Ring Domes which was supplied by Mesa El Nejahuete, and is distributed widely in the northern part of the area. The Lake deposites is deposited on the Tala Tuff within the Caldera lake which was formed by the collapse. The Deposits are mainly composed of sand, pumic tuff and conglomerate, and they can be divided to an upper part which shows remarkable lateral facies change and to a lower part which shows more lithoidal feature consisting of giant pumice, siltstone and sandstone. Thickness of the upper part is

over 50m and that of the lower part is 5 - 30m. A partial Paraconformity is observed in their boundary. Existence of the paraconformity suggests the Lava dome forming and the land making movements of the lake which are connected with upheavals, while the lateral facies change does the volcanism and the movements associated with upheaval and collapse during sedimentation on the Lake. The Lake deposites are called the Arroyo El Caracol Formation in Fig. 2 and 3.

(2) Fracture survey

Fig. 3 shows mappable faults based on a route map (1:2,000 in scale). NE-SE oriented normal faults are dominant and are intersected with lateral separation faults which have NW-SE trend. Furthermore, reverse faults are observed near PR-2. Since these faults systems cut Mesa El Nejahuete Rhyolite, they appear to be formed lates than dome up (50-60 thousands years ago).

How to extend fractures observed on the surface into deep subsurface would be important. Thus, the paleo-stress field was first restored using conjugate minor faults, slicken sides and tensional fractures which were observed at outcrops (for restoration method, see RAGAN, 1968). Fig. 4 shows a paleo-stress field in the geothermal manifestation area. According to the Figure, the maximum principal compressive stress (σ_1) is nearly vertical, while the minimum principal compressive stress (σ_3) is nearly horizontal in the NW-SE direction. It suggests that normal faults can develop easily to the NE-SW direction in this Area. Under consideration of the bending by means of dip direction, anticlines and synclines can be drawn to the NW-SE direction. It

means that minor faults was connected with upheavals and collapses, and its axis of movement had a NW-SE Trend.

Fractures with slickensides and veins are observed in the core taken from the wells. Since the core can not be taken along a definite direction, general discussion on the orientation of fractures is impossible. However, in case of recent rocks which have nearly same geomagnetic fields as that of the present time, the orientation of fractures can be studied by means measuring the remanent magnetization. Accordingly, a temporary magnetic north about 8 cores was defined and sampled from the geothermal wells. The real north has been then determined by measuring the remanent magnetization using astatic magnetometer. Table 1 and Fig. 2 show fracture stress fields which were restored on the basis of this real north. As shown in Table 1 and Fig. 2, the main stress directions, except for PR-2, 1,360m, are harmonized with that obtained on the surface. It suggests that fractures which were found from surface survey would be extended up to the upper part of the Cordilleran Volcanics.(see Appendix)

Now, since the main geothermal reservoir in this area consists of fractures which constitute the lower part of Cordilleran Volcanics, it is the most important to know the characteristics of those fractures. However, the Cordilleran Volcanics are not distributed in this Area. Analyses have been therefore made to interpolate the characteristics and structure of the Volcanics located around Sierra La Primavera Caldera. To the NE of Caldera along Santiago River, the Volcanics contain many fractures with NW-SE, NNE-SSW and ENE-WSW trends, while fractures with NW-SE are

dominant near Santa Rosa Dam in the NW of this area. On the other hand, fractures with NW-SE, N-S and E-W trends are frequently observed to the S and SW of Caldera. Consequently, fractures which are dominant over the entire area have a NW-SE trend. In addition, considering that strikes and dip of Mesozoic located in the W of La Vega have N65-70 W and 50 N trends, and that the arrangement of the Quaternary volcanoes such as Tequila, Tepetiltic and Sierra La Primavera Caldera is in NW-SE direction. Volcanism in the area is assumed to be provided through fractures with NW-SE trend in deep subsurface.

MAHOOD (1980) has pointed out that the center of the area has the highest structural contour line of the lowest horizon of the giant pumice, suggesting that the summit of the resurgent uplift after caldera forming is located in some where near here. By assuming that anticlinal bending restored by stress field were formed from this uplift, conjugate shear faults might be easily built near the surface where the influence of uplift is less significant, while high angle extensional fractures might be easily built in the deep subsurface where the influence is more significant. Large scale lost circulations in Wells PR-1, 5 and 8 are caused by these extensional fractures. Some conjugate shear faults with geothermal manifestation such as hot spring and fumarole are supposed to be connected with these extensional fractures.

Fig. 5 shows tensional fracture distributions on the surface. They are well developed between PR-1 and PR-8, conforming with the anticlinal bend structure assumed by minor fault analy-

sis. Fig 6.indicates the orientation of tensional fracture in the Tala Tuff with random direction. So that, the fracture also includes that of thermal stress origin which was caused by cooling stage of pyroclastics.

(3) Surface alteration survey

This survey was mainly carried out on the fumarole site. Following the observation of fumarole distributions and alteration characteristics in the site, 82 samples as representative altered rock have been analysed by means of powder X-ray diffraction method to identify the alteration minerals, and the alteration zones were defined at the same time.

The identified alteration minerals are Quartz, Cristobalite, Tridymite, Kaolinite, Halloysite, Montmolrillonite, Sericite, Alunite, Gibbsite and Pyrite. Of these minerals, the zone are called Kaolinite zone and Alunite zone respectively where these 2 minerals recognize.

As shown in Fig. 7 most of acid alterations with fumarole are in the Kaolinite zones. They are mainly distributed in the vicinity of PR-5 and PR-8, showing NE-SW trend. The Alunite zones show very limited distributions with occurence enclosed by the Kaolinite zone in ca.150m NW of PR-8 and in E ca.200m of PR-2.

(4) Study on cores and cuttings

Fig. 8-11 show the study results on cores and cuttings from existing wells. The following are some important points.

First of all chemical analysis of Hg and As from the cuttings sampled at more than 1,000m in Wells PR-1, PR-2 and PR-8 shows that these elements significantly affect the subsurface

fractures, i.e. in case of PR-1 high Hg and As concentration at 1,630m corresponds to a lost circulation at ca.1,620m. Also high concentration of Hg and As at 1,490m reflects probably a complete lost circulation at 1,445m. In PR-2, Hg concentration increases with the depth over ca.1,950m and that of as over ca.1,800m. Such concentration trends reflect small continuous lost circulation which appeared at more than 1,822m. Hg and As concentrations in PR-8 show a similar tendency. Peaks are observed at 1,340m, 1,460m, 1,560m, 1,610-1,690m, 1,740m and 1,810-1,850m. These correspond to the lost circulation at 1,328m, 1,436m, 1,564-1,569m, 1,640-1,643m, 1,752m and 1,790-1,793m respectively. Furthermore, as high concentration at ca. 1,130m seems to reflect the lost circulation at ca. 1,100m. As mentioned above, Hg and As were especially useful for fracture assessment. The reason of it is that Hg and as originated in volcanism are concentrated and stored in the fractures.

When the hot water penetrates into igneous rocks, the Magnetite transforms easily into the Pyrite. Accordingly, under the assumption that the magnetic susceptivity decreases with higher permeability, the magnetic susceptivity was measured at the depth more than 1,000m in Wells PR-1, PR-2, PR-8 and RC-1. The results show a good conformity of the low susceptivity with lost circulations during drilling of Well PR-8. However, in case of other wells, it is corelated with the lithology, i.e. new rocks show a higher susceptivity, while white clay alteration zones show a lower one.

Subsequently, Quartz, Calcite and Amkerite were selected out

from cuttings in PR-1, PR-2, PR-5, PR-8 and RC-1, because these minerals are suitable to determine the homogenization temperature of fluid inclusion. Results of the measurement using heating microscopy for each well are as follows:

PR-1: The minimum homogenization temperature at the depth less than 1,100m is nearly same as the static downhole temperature (Standing time ST:408 hr.), whereas the homogenization temperature becomes lower by 42-45 ℃, than downhole temperature indicating a value of 260-284 ℃ as the minimum homogenization temperature at the depth more than 1,500m. A coexistence of both gaseous inclusions and liquid inclusions was observed, resulting in an assumption that a part of geothermal fluids produced a boiling in the initiation phase of inclusions.

PR-2: The minimum homogenization temperature increases with the depth, slowly i.e. from 118 ℃ at 680m to 150 ℃ at 1,780m. But the increase in temperature becomes abruptly at the depth more than 1,780m, showing 240 ℃ at 1,985m near the bottom.

PR-5: Cuttings were missing at the depth more than 895m, measurement was thus carried out up to this depth. The minimum homogenization temperature increased drastically from 104 ℃ at 350m to 144 ℃ at 580m. Then some decrease trend was observed up to 750m, followed by a steep increase from 750m to 800m.

PR-8: At the depth of ca. 1,800m where is a main feed point, downhole temperature decrease was observed. Except for this depth and 1,250m, both the borehole temperature curve and the minimum homogenization temperature curve for fluid inclusion show a same phase. Further, the both values are fairly similar at 1,630m. It

is concluded from the above observation that the distribution of the minimum homogenization temperature would be close the that of subsurface temperature before drilling. The highest value of the minimum homogenization temperature is 292 ℃ at 1,790m. It is assumed, as in case of PR-1, that this Well also encountered a partial boiling of the geothermal fluid in the initiation phase of inclusions.

RC-1: The minimum homogenization temperature increases slowly from 78 ℃ at 890m to 122 ℃ at 1,855m. The highest value amounts only 122 ℃ at 1,855m. From the analysis results of cores sectional distribution of the minimum homogenization temperature for the wells, it is very probable that the geothermal fluid upflows along deep-seated fractures in PR-1, PR-8 and PR-5 zones (Fig. 12).

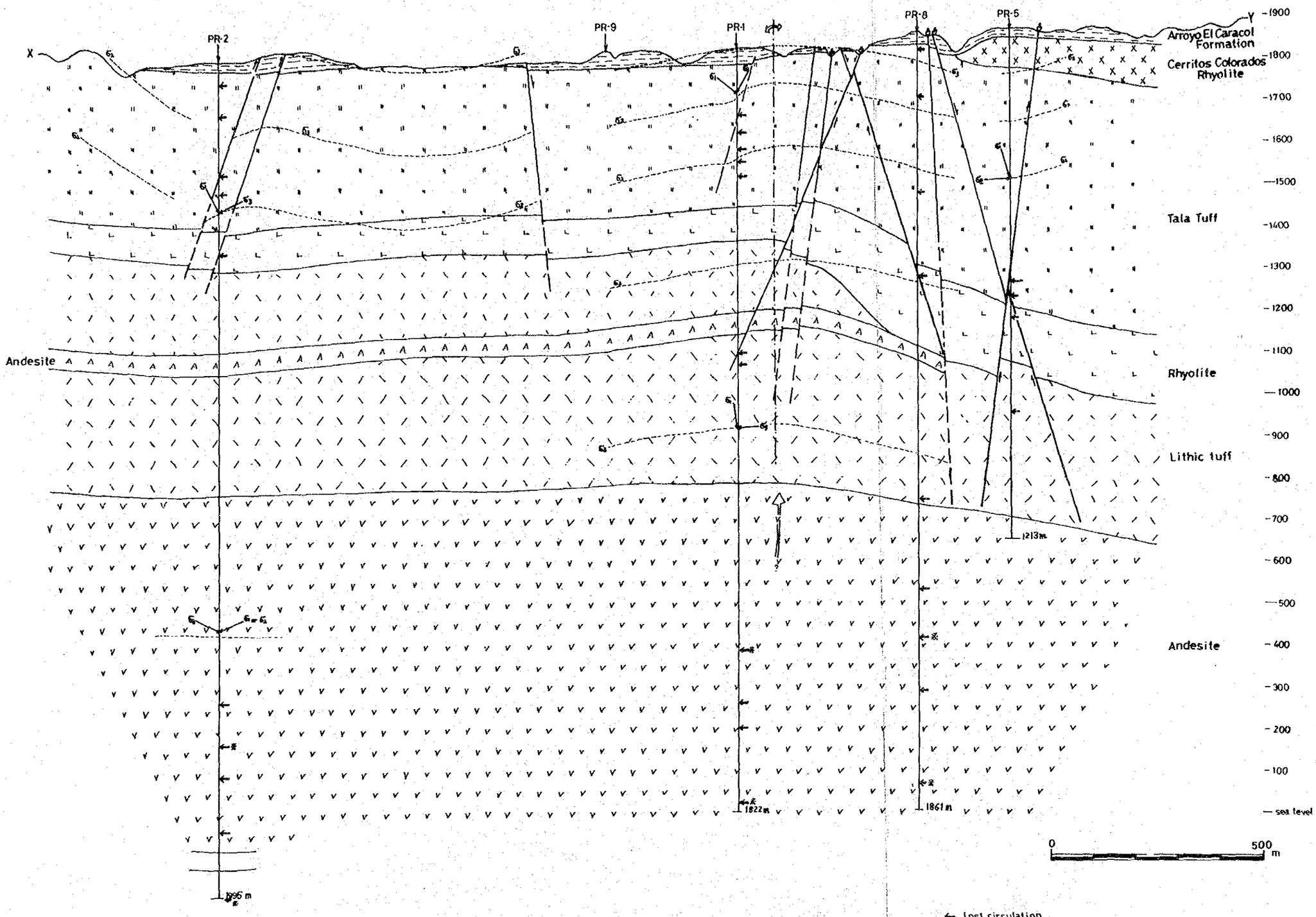

Fig. 2. Geological profile and stress trajectory

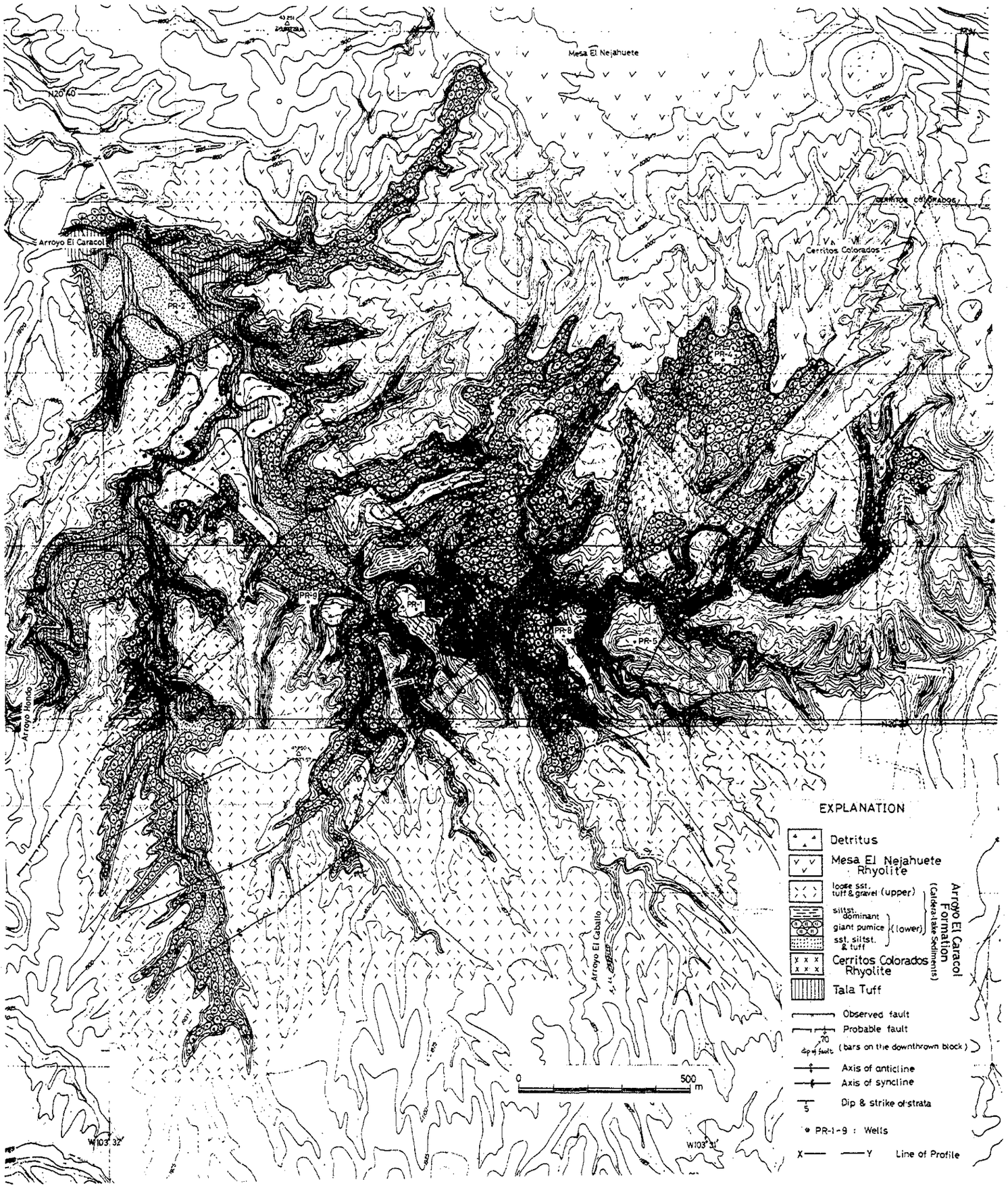

Fig. 3. Geological map

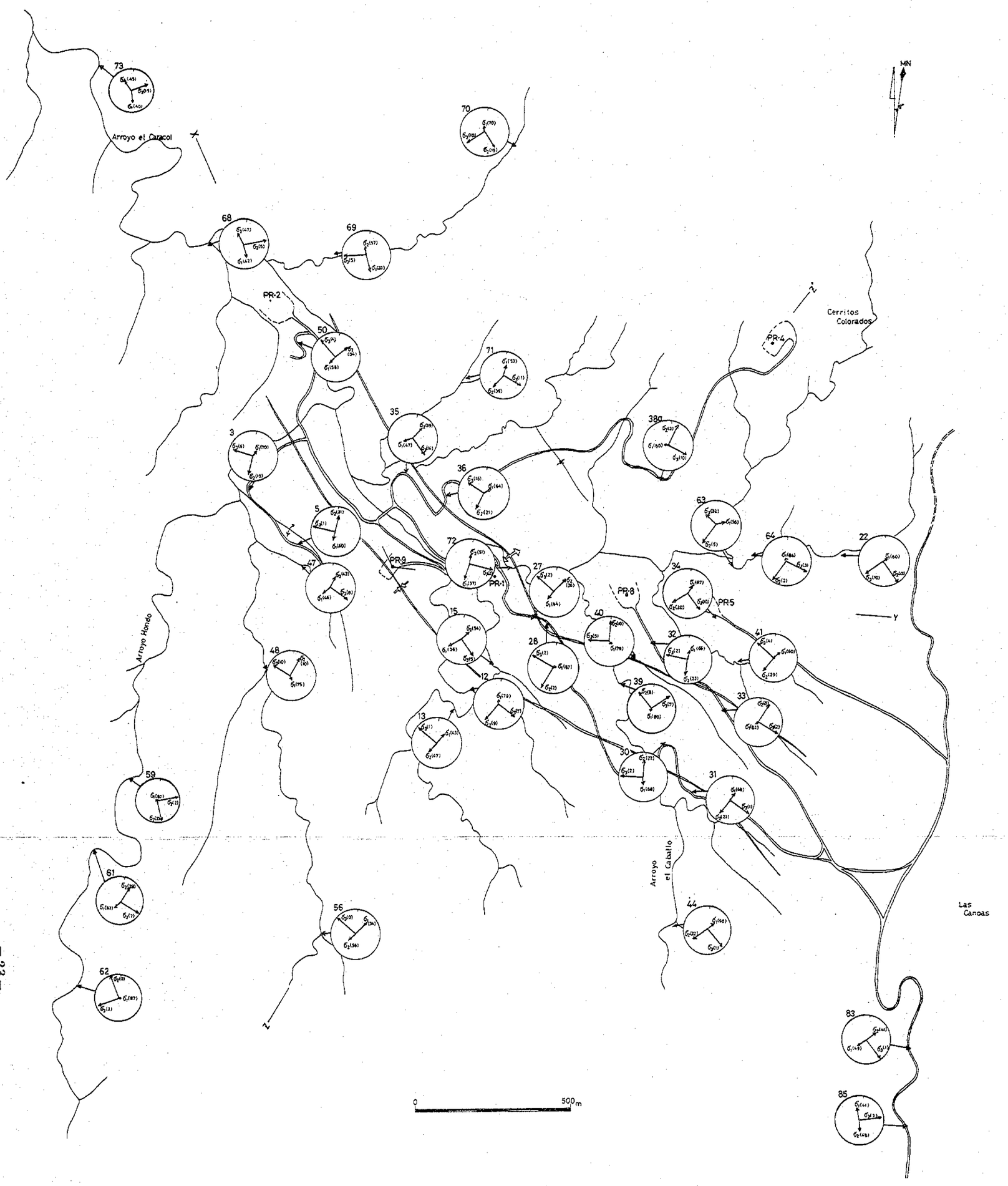

Fig. 4. Principal stress axis of each measuring point
σ_1 : maximum principal stress axis

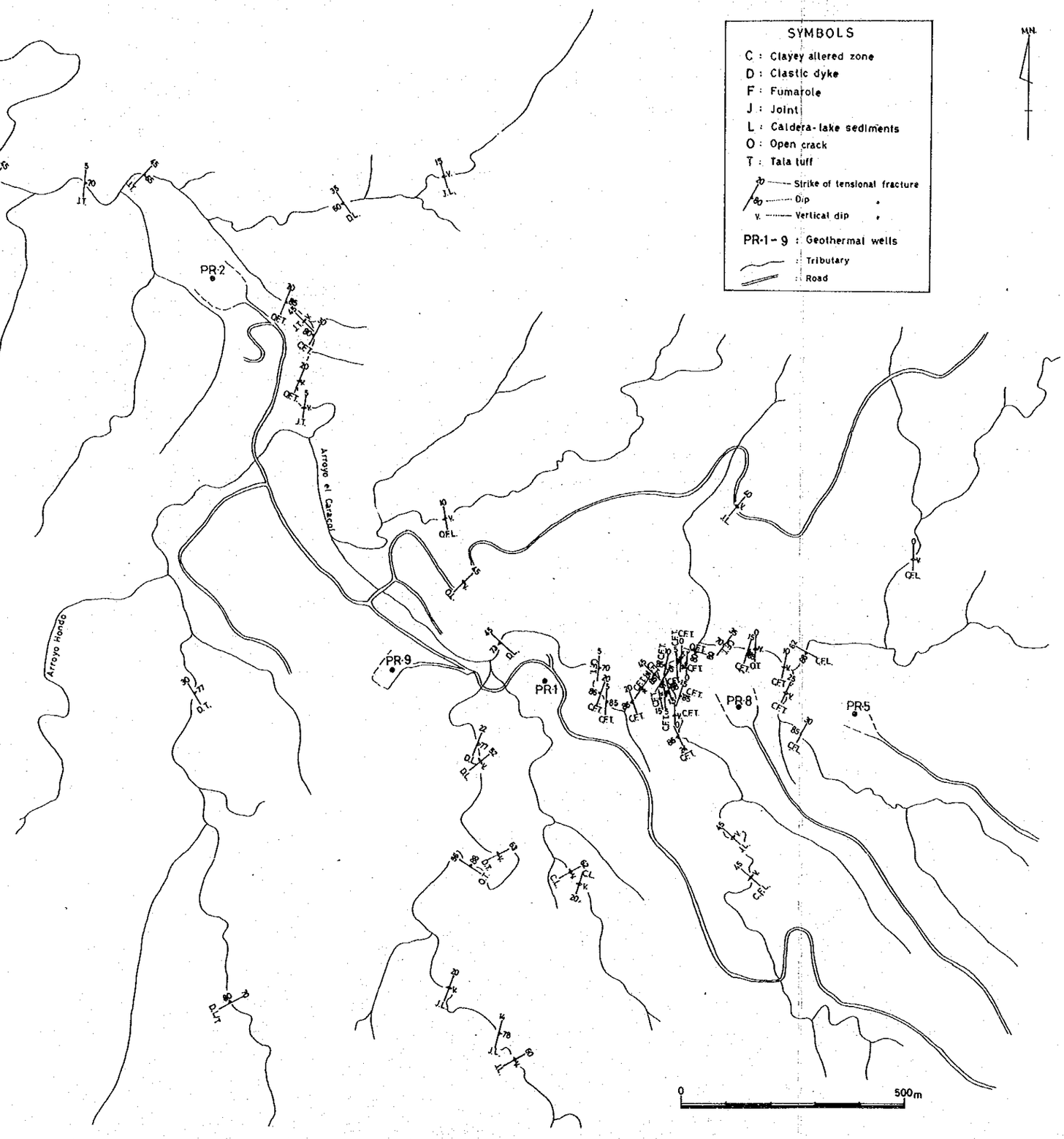

Fig. 5. Tensional fracture map

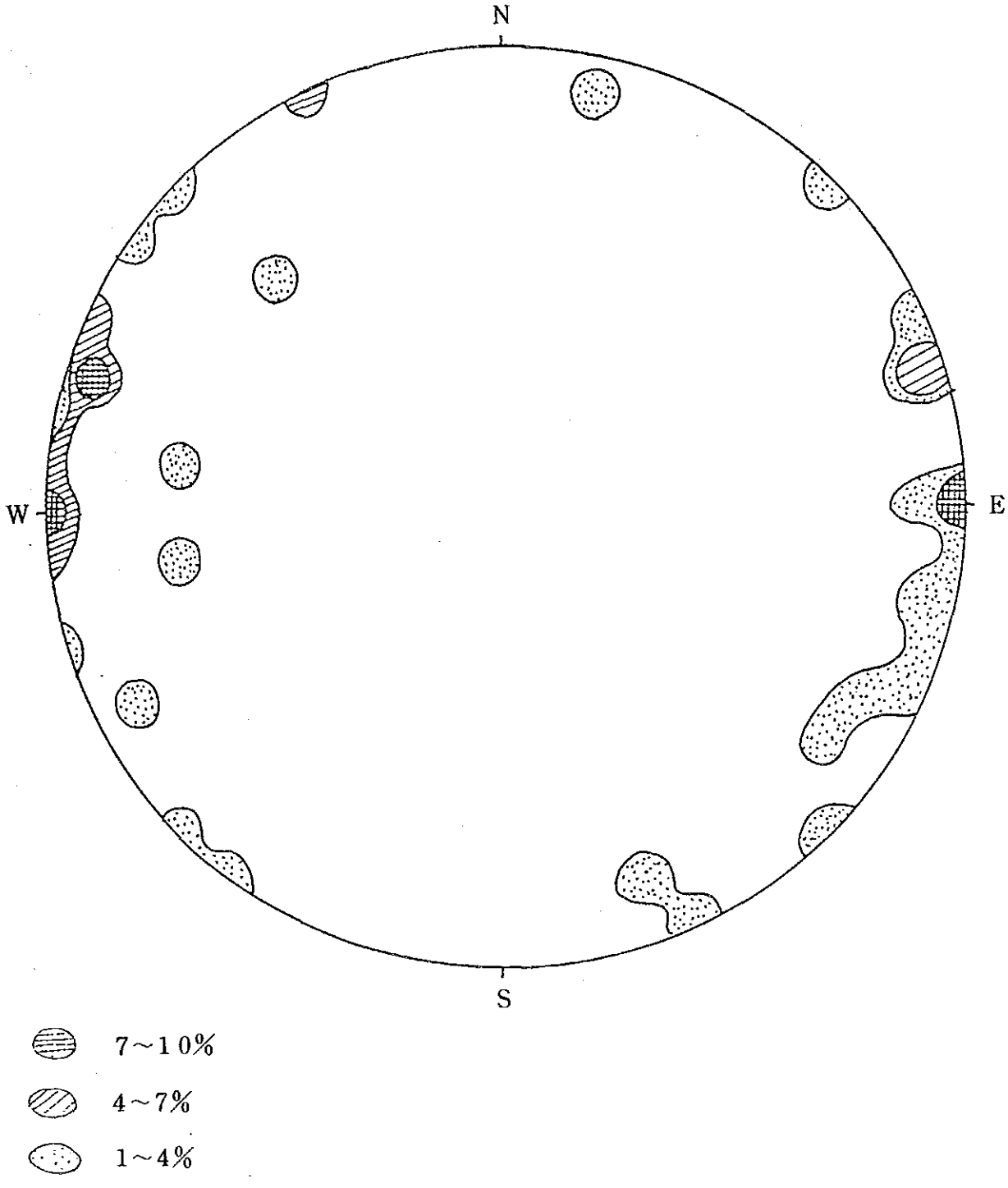

Fig. 6. Orientation of tensional fracture in the Tala Tuff at 35 measuring points

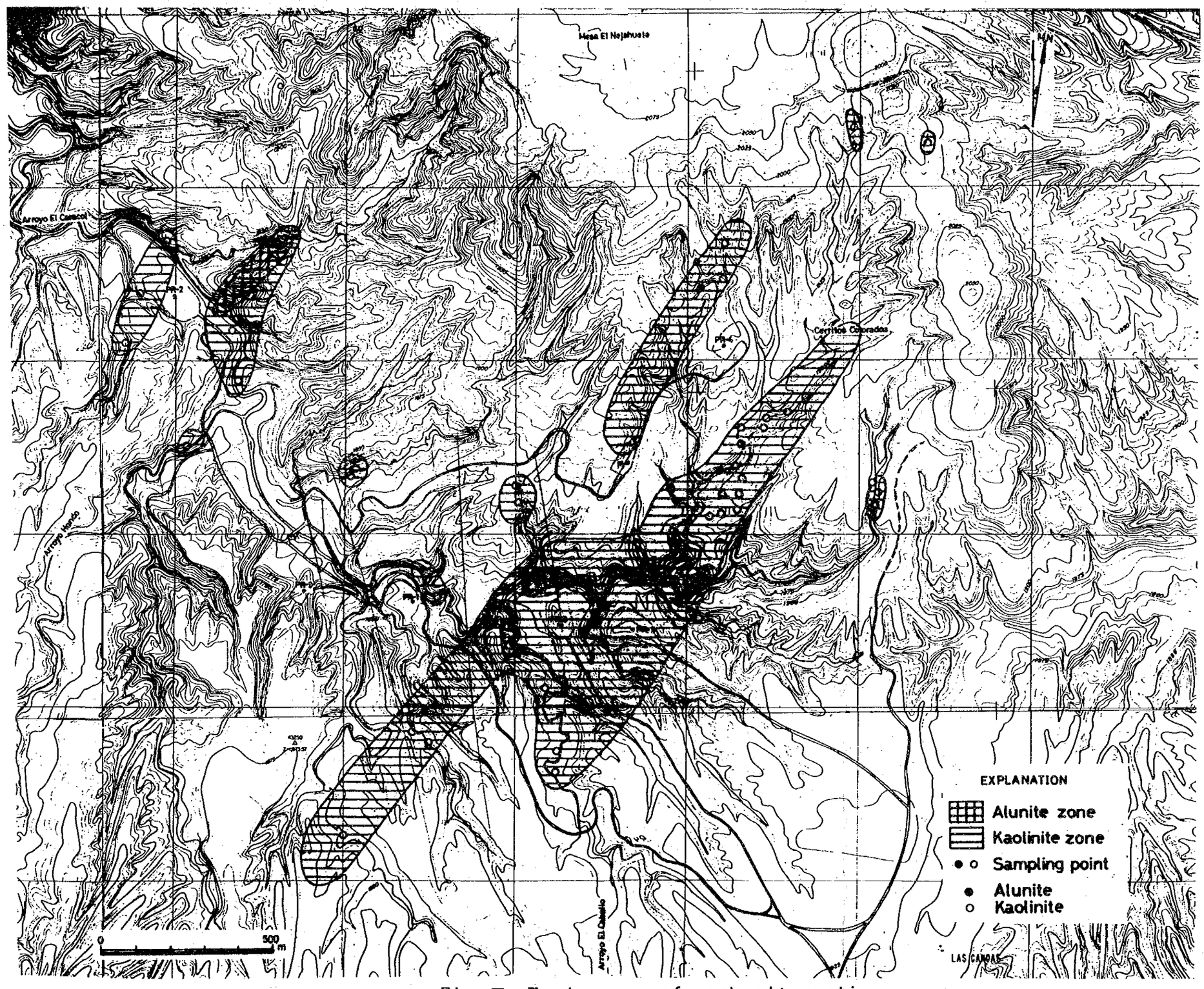

Fig. 7. Zoning map of rock alternation

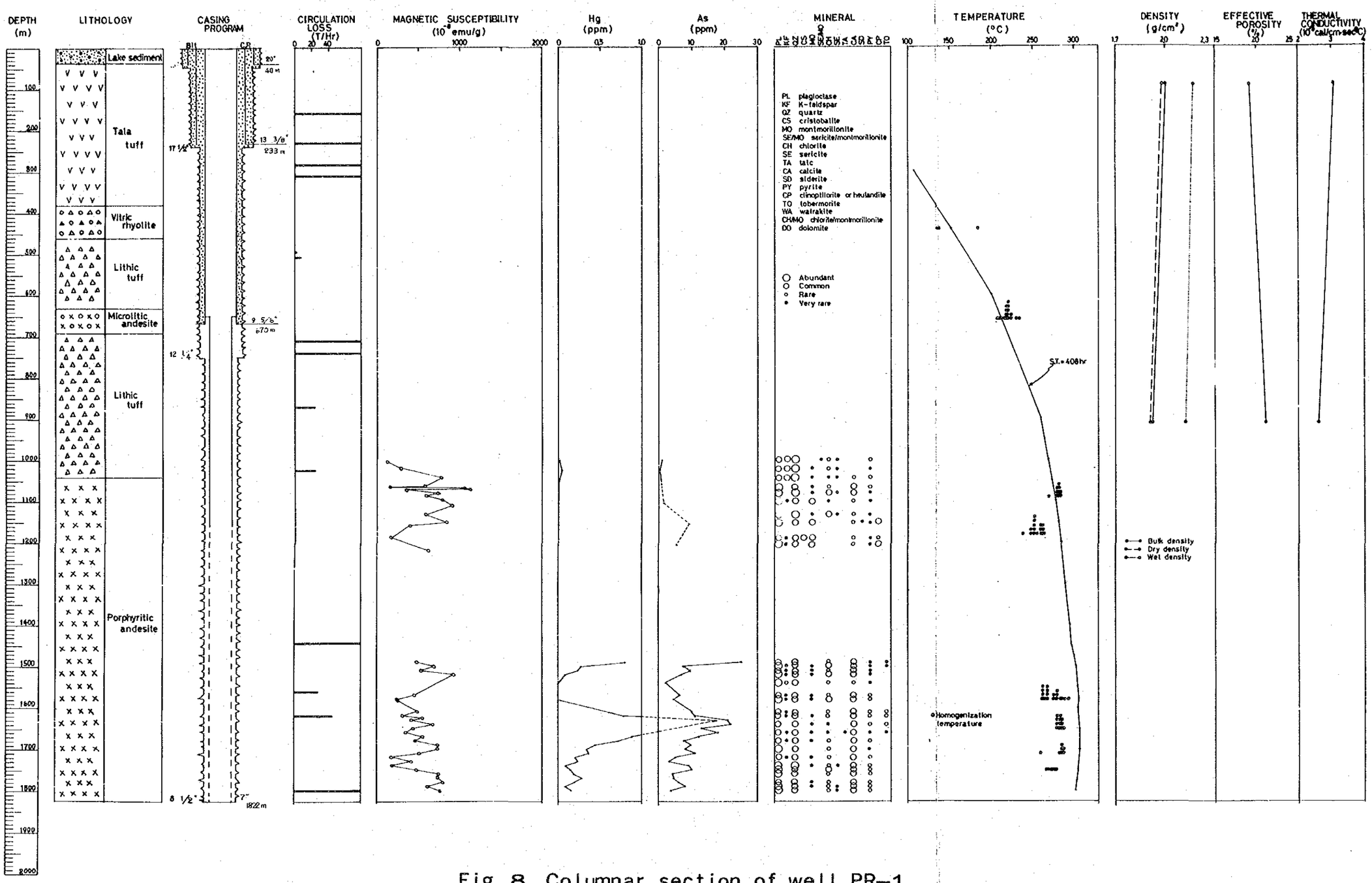

Fig. 8. Columnar section of well PR-1

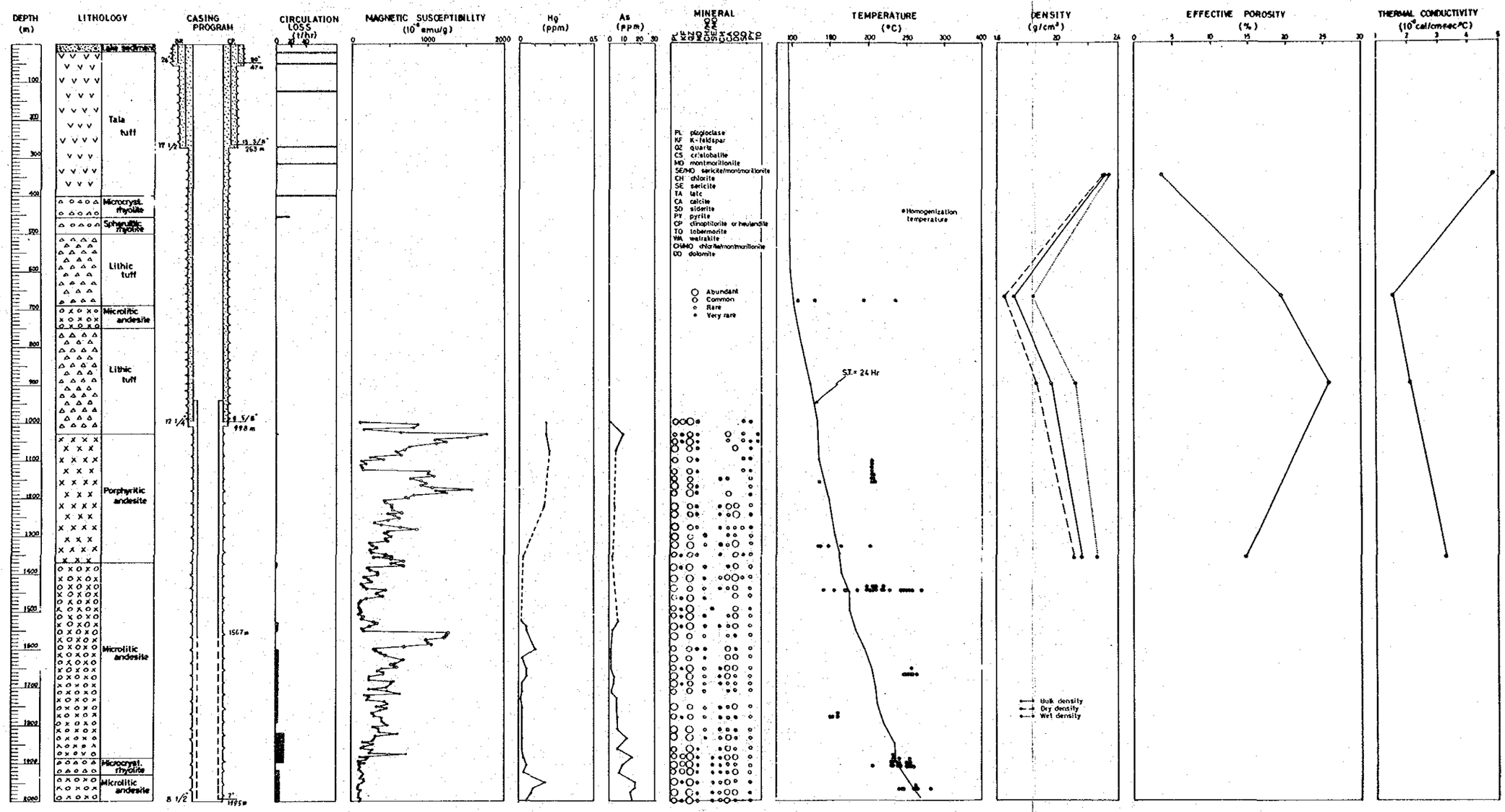

Fig. 9. Columnar section of well PR-2

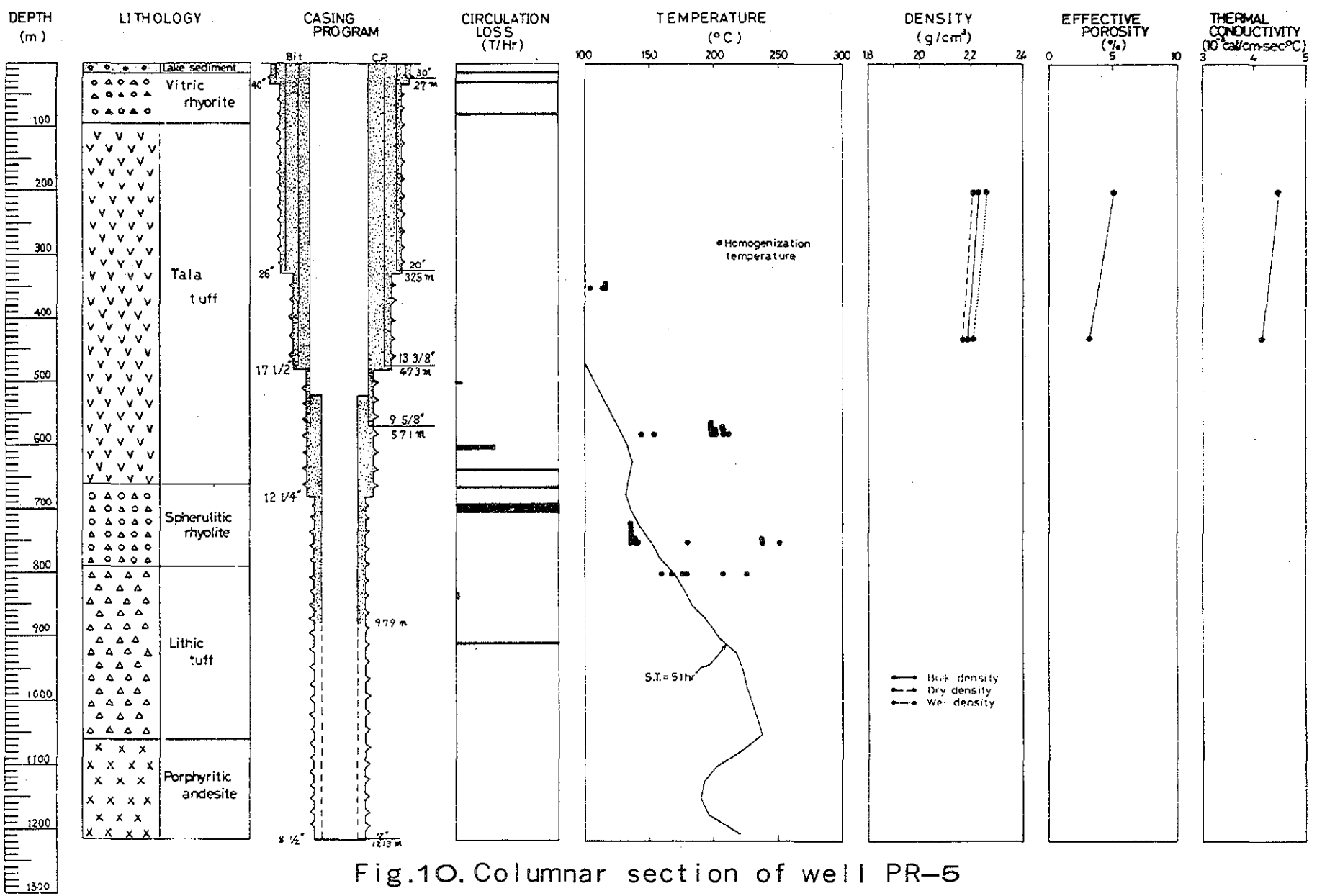

Fig.10. Columnar section of well PR-5

WELL PR-8

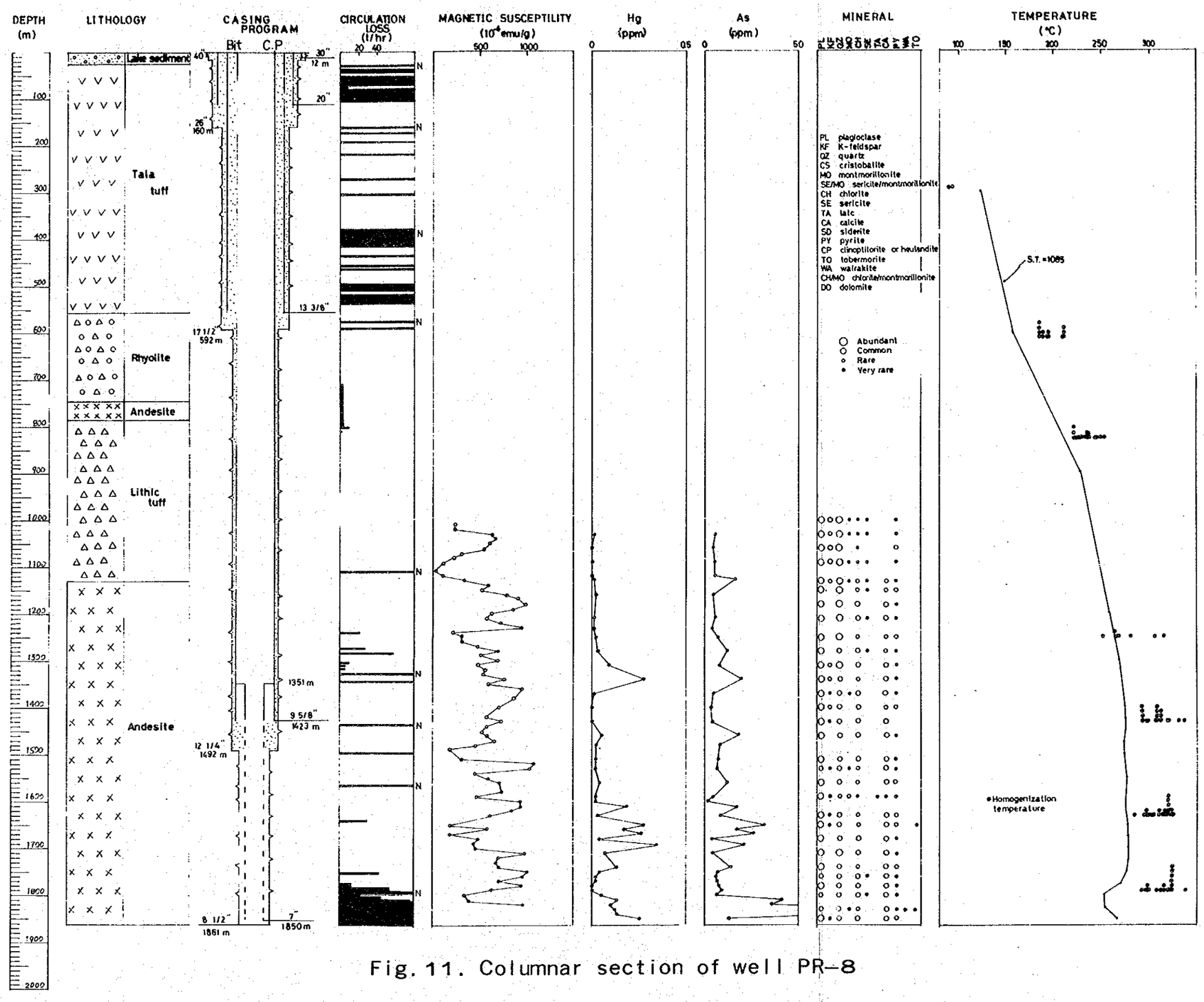

Fig. 11. Columnar section of well PR-8

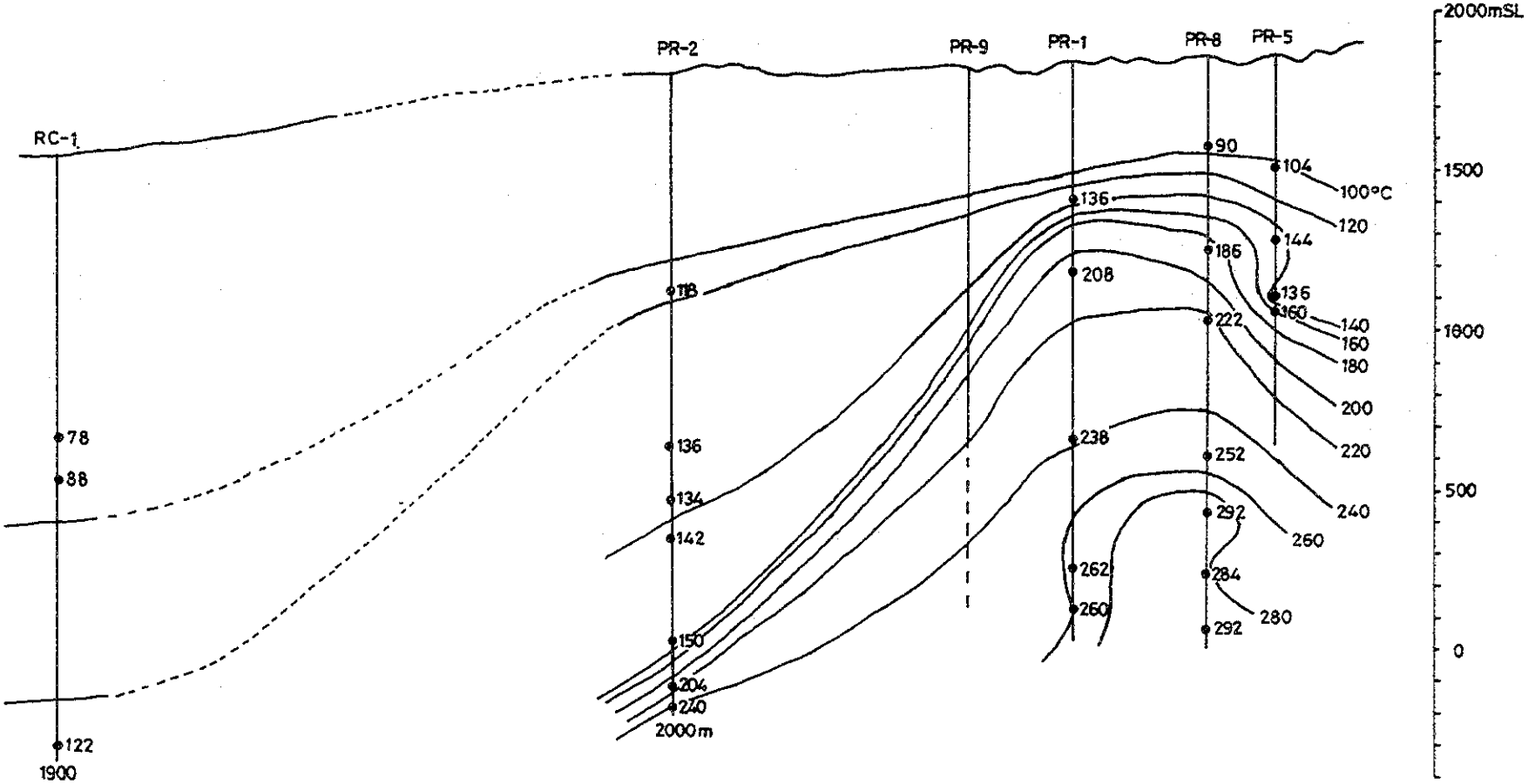

Fig. 12. Profile of minimum homogenization temperature

Table 1. Remanent Magnetization of cores

	Well number Depth of core Rock name	Demagne-tization mT	Strength of magnetization KA/m×10^{-3}	Declination of assumed north (Clockwise)	Strike, dip and slip direction of fracture	Principal stress axis
1	PR-1 93m Welded tuff	0 10 20 30	2.25 2.25 2.21 2.00	259° 259 260 258	Vein N70° W 32° NE	σ1:N82° E. 30° W σ2 N82° E. 60° E σ3 N8° E. 0°
2	PR-1 910m Welded tuff	0 10 20 30	2.29 2.31 2.28 2.09	231° 230 228 230	Slicken-side N30° W 63° S 80°	σ1:N56° E. 84° W σ2:N22° E. 5° NE σ3:N69° W. 3° E
3	PR-1 915m Welded tuff	0 10 20 30	1.49 1.52 1.50 1.43	170° 170 169 168	Slicken-side S4° W 64° N 87°	σ1:N60° E. 86° W σ2:N11° W. 2° N σ3:N78° E. 3° E
4	PR-2 350m Welded tuff	0 10 20 30	2.95 2.90 2.21 1.22	108° 107 108 109	Slicken-side N40° W 30° N 90°	σ1:N19° W. 60° S σ2:N71° E. 0° σ3:N19° W. 30° N
5	PR-2 1360m Andesite	0 10 20 30	7.47 6.86 5.43 3.49	61° 59 65 70	Vein S37° W 90° lateral separation is N53° E	σ1:N81° W. 38° E σ2:N46° E. 38° SW σ3:N18° W. 29° N
6	PR-4 300m Welded tuff	0 10 20 30	4.17 3.51 2.86 2.26	19° 19 18 17	Vein N10° E 85° SE	σ1:N58° W. 85° E σ2:N63° E. 5° W σ3:N27° E. 0°
7	PR-5 350m Welded tuff	0 10 20 30	4.17 3.43 2.58 2.07	85° 88 88 85	Slicken-side NS 80° E 90°	σ1:N 5° W. 70° N σ2:N85° E. 0° σ3:N 5° W. 20° S
8	PC-1 700m Andesite	0 10 20 30	9.24 9.18 8.63 7.12	198° 198 199 198	Slicken-side N37° W 54° S 60°	σ1:N36° W. 74° S σ2:N 8° W. 15° N σ3:N81° E. 3° W

II-2 Geochemical survey

The first geochemical survey is mercury concentration analysis is soil of 272 points within the extent of 9.6 km² including the well site area existed. The second geochemical survey is chemical and isotopic analyses of wellbore fluids from PR-1 and PR-8 which have already drilled by C.F.E. Steam and condensed water of geothermal fluid were collected after separating from hot water by using a small-scale separator set up a line pipe through the well. Hot water was collected under the atmospheric condition.

(1) Mercury survey in soil

Enclosing the geothermal manifestation area at the center, 272 points were set up within a network (area: 9.6 km²) with borderlines of 3.2 km length to E-W and of 3.0 km to N-S. At each point, soil sample was taken from 1m depth to determine the Hg concentration (Fig. 14). Table 2 shows the Hg analysis results. Determination was made on the air dried samples.

A distribution diagram of Hg concentration accumulative frequency (Fig. 13) is propared based on the results. According to the diagram, Hg concentration can be divided into 2 groups with boundary of 70 ppb. In other words, there are 2 mechanisms for Hg rise. Of these mechanisms, higher concentration would be resulted from ascent through fractures, while the lower one shows a gradual accumulation through pores in the formation. Finally the Hg concentration are divided into 5 steps with boundaries of 18, 32, 70 and 178 ppb according to the above consideration. A distribution map is prepared in Fig. 14. As shown in Fig. 14, the

points which indicate higher concentration with 70 ppb or more are mainly located in the eastern part of the area. There are several zones where significantly crowded points of high concentration can be observed. High concentration points in the east of the area shows a line arrangement with NE-SW orientation, although these points are not always distributed continuously. According to Fig. 14, the distribution of Hg high concentration points and that of natural fumarole show a similar NE-SW orientation with overlapped locations in the eastern part of the area. Consequently, it would be presumed that there are fractures of NE-SW trend producing natural fumarole and high Hg concentration in this area.

On the other hand, natural fumarole and high Hg points surrounding PR-2 show a discontinous and isolated distribution compared with that of the east, resulting in assumption that no fracture exists in a large scale in this area.

(2) Chemical analyses of wellbore fluid

Steam, condensed water and hot water from PR-1 and PR-8 were chemically analysed, followed by a consideration on the geothermal reservoir mechanism based on their chemical characteristics. Table 3 shows the chemical analysis.

On purpose to estimate the temperature of the geothermal fluid, the geochemical temperature has been determined using 4 types geothermometer (Table 4). They are the solubility of Quarts (adiabatic cooling), 2 types of Na/K ratio proposed separately by 2 authors and Ca corrected Na/K ratio. The values from these 4 geothermometers are nearly same for PR-1, while those for PR-8

shows a remarkable dispersion. Taking into account that the reaction rate of Quartz dissolution will increase above 250 ℃ and the reequilibrium will take place during fluid flow-up in the wellbore, the fluid temperature in PR-8 might be more than 274 ℃. The value of Na-K-Ca thermometer seems, therefore, to be reasonable.

According to the well test results, the downhole temperatures are 299 ℃ at 1,800m for PR-1 and 235 ℃ at 1,800m for PR-8. A finding is already known that in both wells the fluid is flowing up under dual phase condition after flashed in the formation, but a certain water level was confirmed near the bottom of PR-1. In case of PR-8, the difference from the geothermal temperature seems to be caused by flashing in the formation.

The relation of the enthalpy with Cl^--concentration of deep hot water (values from Na-K-Ca thermometer with flash correction) was, then, studied to guess flow conditions of underground (Fig. 15). Data on PR-2, PR-4 and PR-5 were given by the results from C.F.E. As shown in Fig. 15, the values on PR-1, PR-8, PR-5 and PR-5 are standing on a line. It suggests that the hot water which originates in the deep formation near PR-1 is contaminated with water whose enthalpy and Cl^--concentration are low while flowing through PR-8 and PR-5. Since a existence of fractures with NE-SW trend was confirmed extending from PR-8 and PR-5 to PR-4 based on a soil mercury and geological survey results, fluid circulation via these fractures can be possible. In addition, PR-4 can be strongly influenced by mixing of surface water because of it's less depth of 600m. Chemical characteristics of hot

water in PR-2 are different from those in other wells. The results of soil mercury survey show no existence of high concentration area between PR-2 and PR-1, PR-8 and PR-5. Thus, an independent hot water reservoir might exist in case of PR-2.

An isotopic composition diagram was prepared to study on the origin of water and it's flow mechanism, as shown in Fig. 16. A straight line in this diagram shows the value of surface water expressed by equation $SD = 8 \times S^{18}O + 10$ (Craig, 1961). In addition to the isotopic composition of hot waters from PR-1 and PR-8, values of hot spring water surrounding the area were given from the analysis by C.F.E. Concerning $S^{18}O$ values, those of PR-1 and PR-8, in particular of PR-1, show high values. It would be attributed to the "Oxygen Shift" which makes a higher $S^{18}O$ value of hot water due to an oxygen isotope exchange with rocks, leading to a conclusion that the hot water in PR-1 has clearer characteristics which is typical for deep subsurface compared with those in PR-8.

Finally, a verification was made on He, Ar and N_2 in steam. Fig. 17 shows clearly that nearly same ratios He/Ar and N_2 /Ar were obtained from PR-1 and PR-8. (He/Ar)s/(He/Ar)air and (N_2 /Ar)s/(N_2 /Ar)air are normalized values of ratios He/Ar and N_2/Ar in the sample by utilizing the atmospheric values. The value from Hervores de la Vega, a hot spring in the neighborhood, is close to the mix-line which consists of the values from PR-1 and PR-8 and of the values from surface water balancing with the atmosphere (points marked with "diss, air"in the diagram). Accordingly, the deep gas in this area, after mixing with the atmosphere

dissolved in the surface in various ratios, is discharged as geothermal gas. The gas from the wells of La Primavera seems to be closer to the deep gas compared with the hot spring gas.

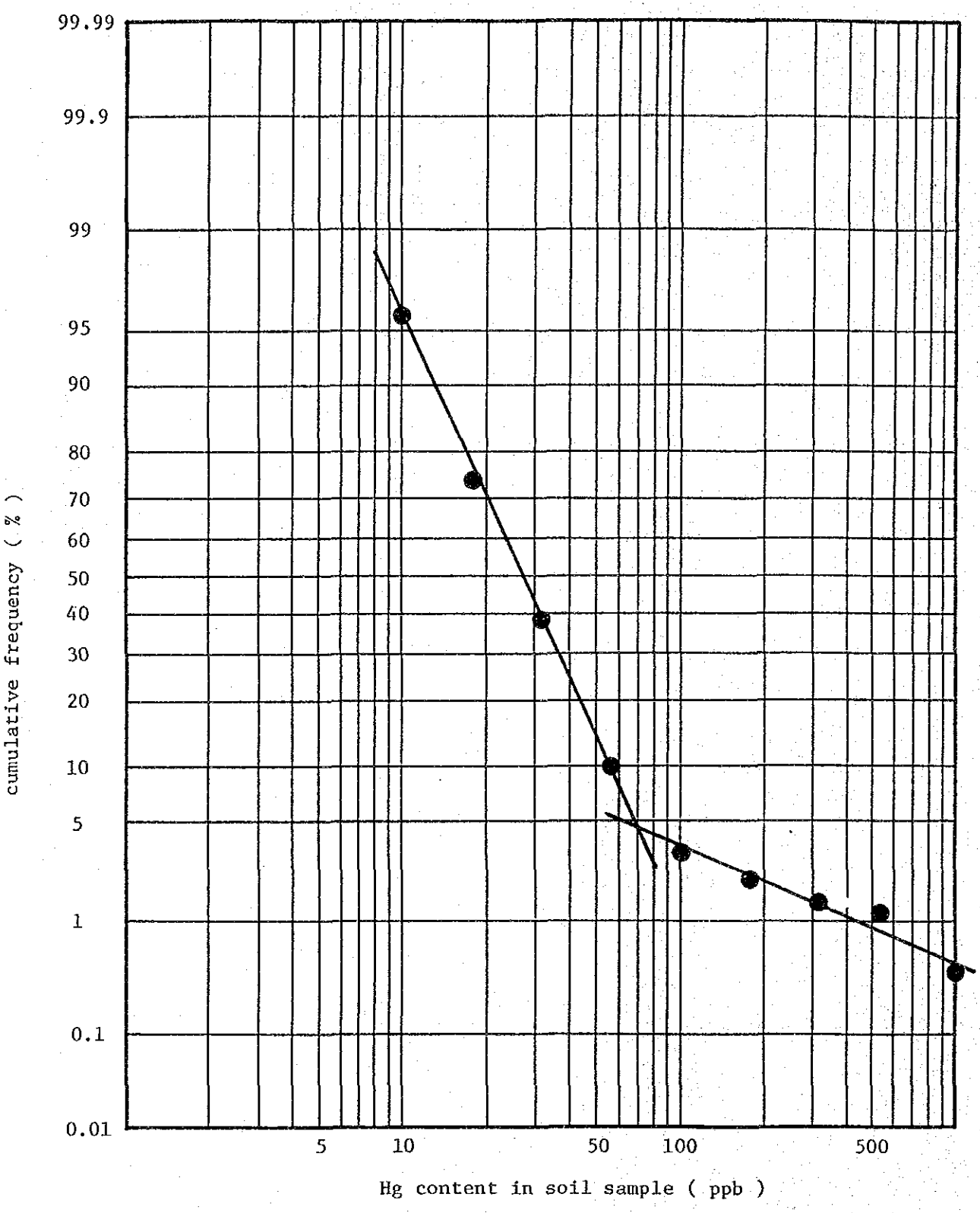

Fig. 13. Cumulative frequency of Hg content in soil sample

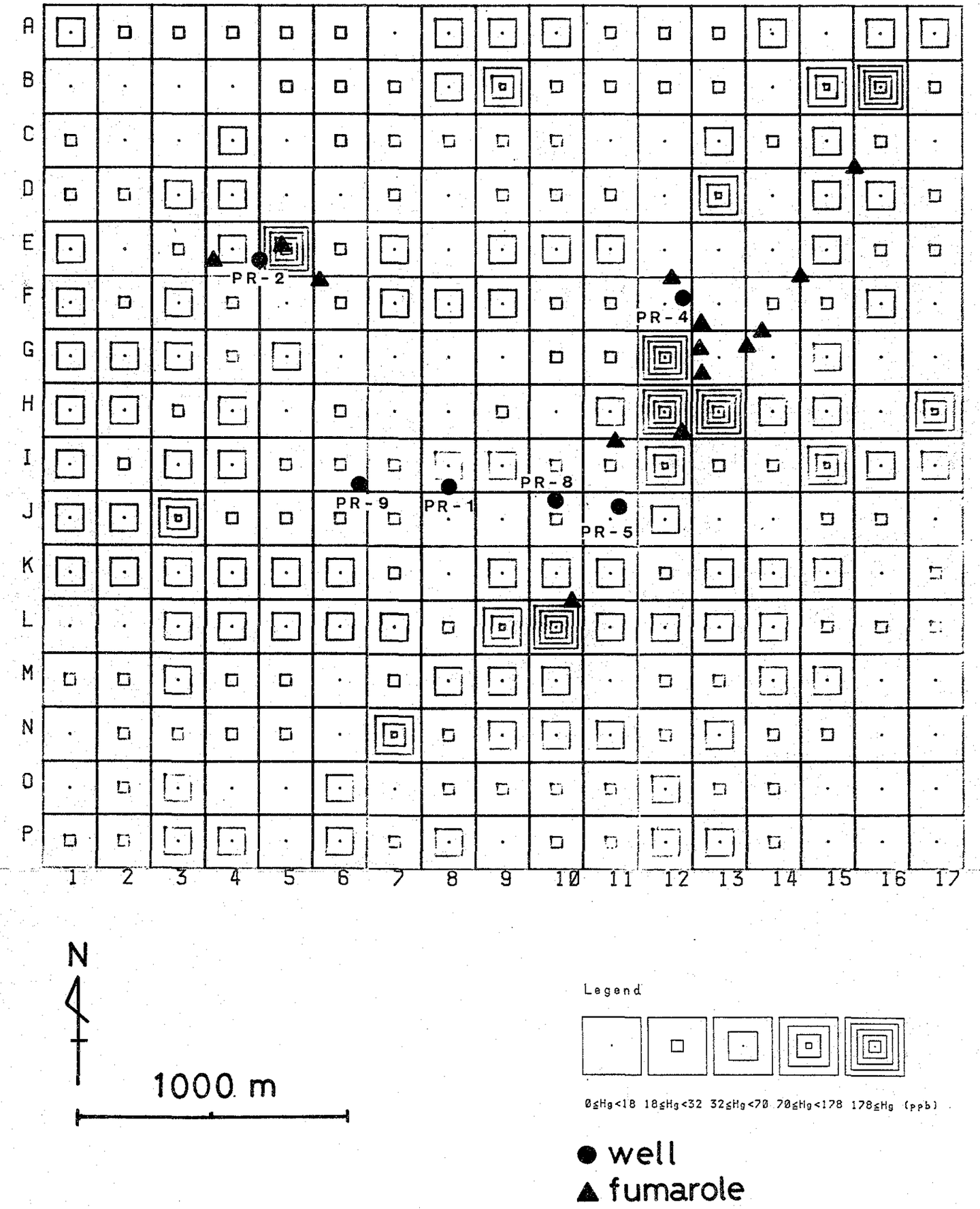

Fig. 14. Distribution map of Hg concentration in soil

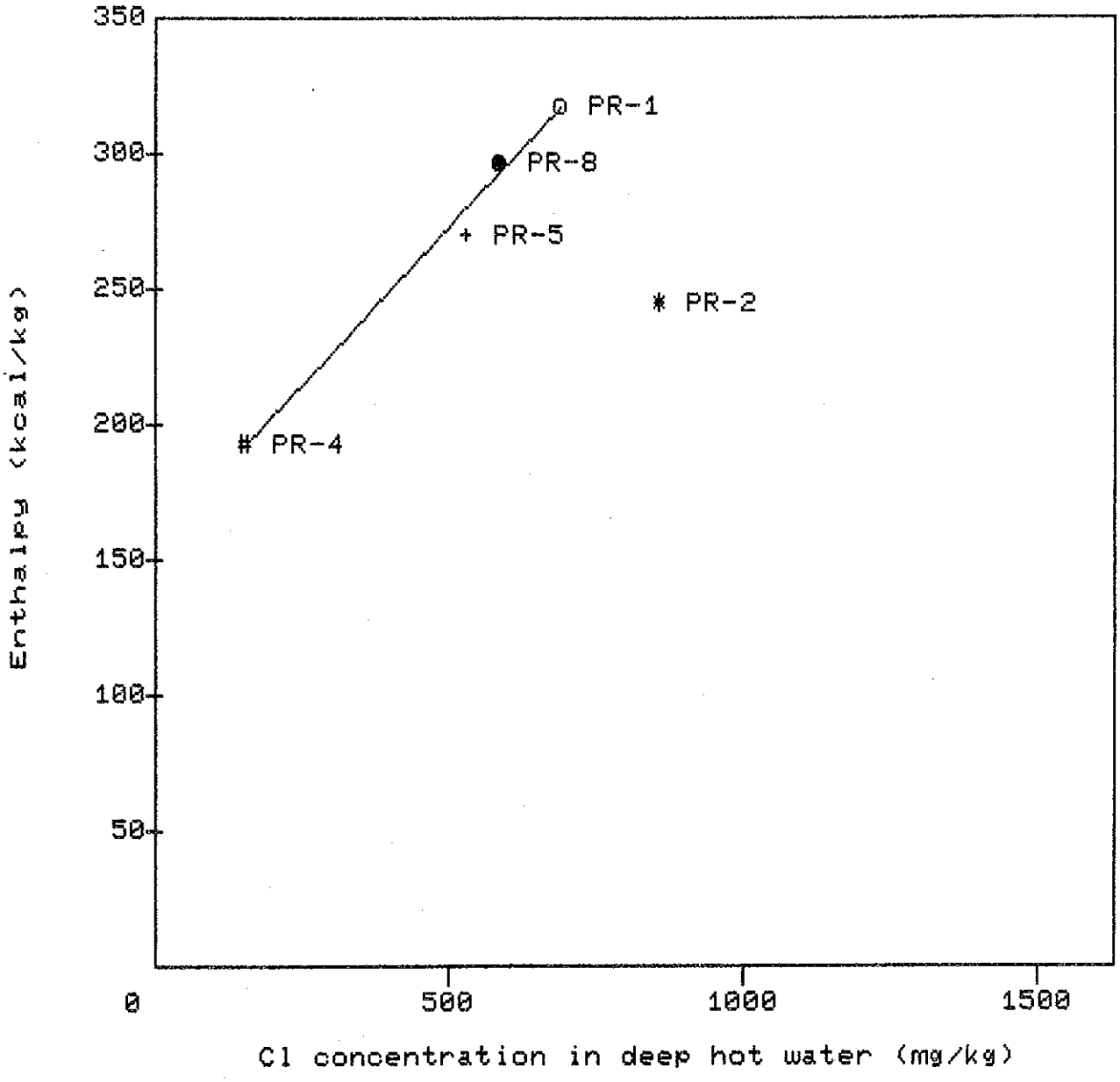

Fig. 15. Relationship between enthalpy and chloride concentration in deep hot water

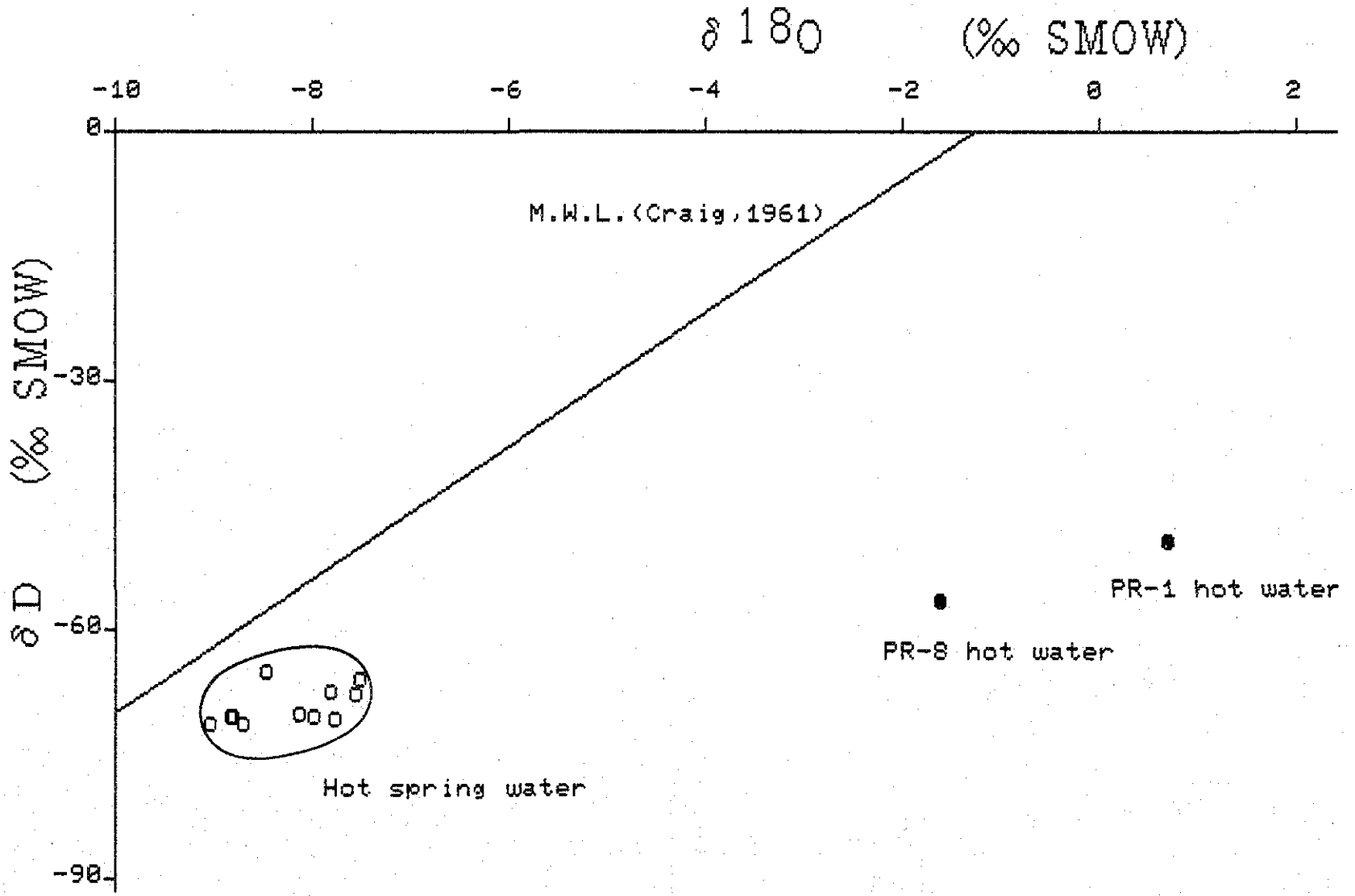

Fig. 16. Oxygen-18 and Deuterium compositions of PR-1, PR-8 hot water and hot springs

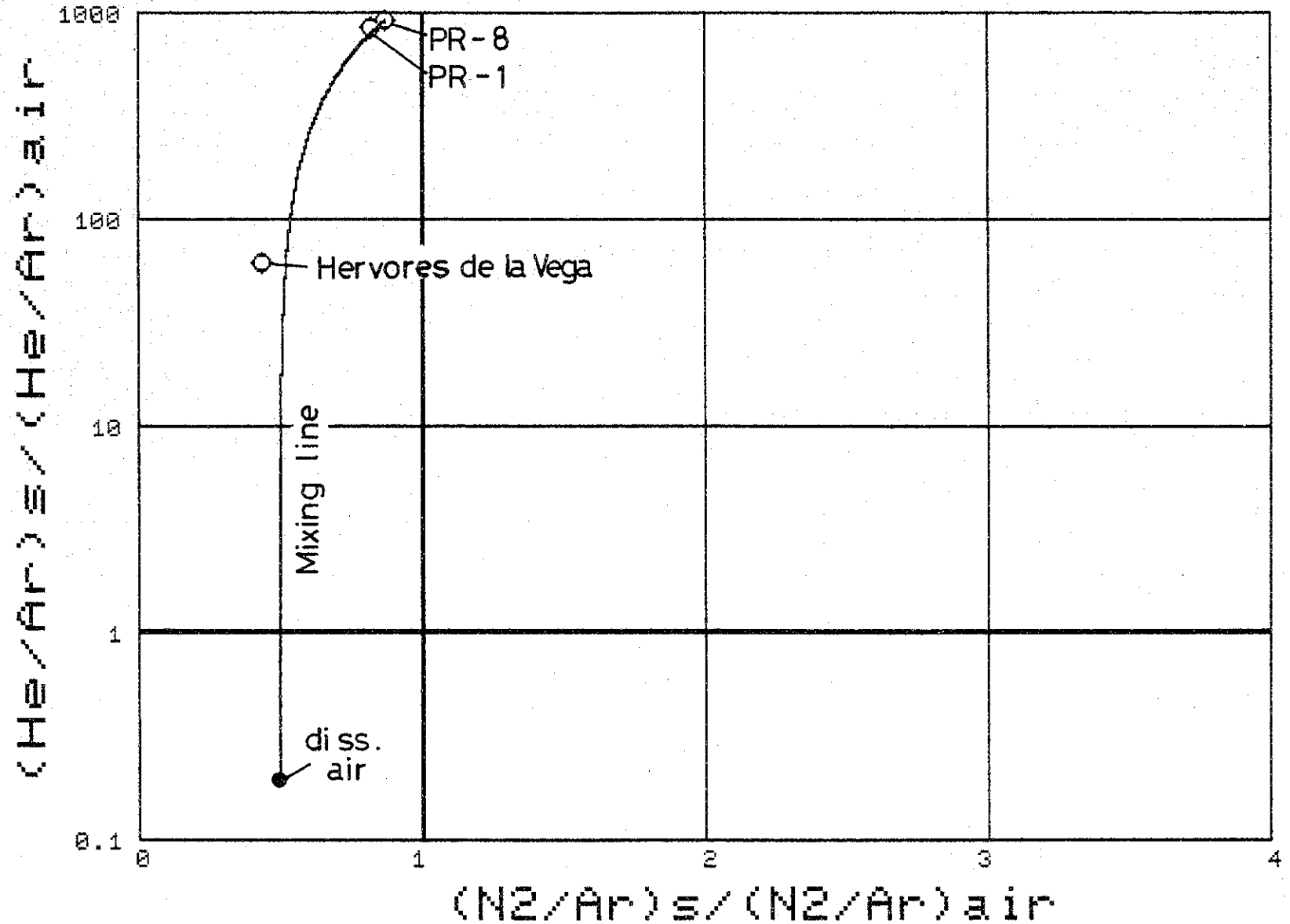

Fig. 17. Relationship between He/Ar and N_2/Ar ratio in geothermal gases discharge from PR–1 and PR–8

Table 2. Mercury concentration value in soil

(ppb)

	1	2	3	4	5	6	7	8	9	10	11	12	13	14	15	16	17
A	35.8	20.5	19.9	19.2	20.0	27.7	11.3	34.8	32.8	39.4	26.4	24.9	18.1	35.1	13.9	34.9	32.6
B	15.2	14.2	10.5	7.0	31.6	21.7	20.1	34.1	87.1	21.4	30.5	22.3	23.8	16.8	123	429	18.1
C	24.2	14.6	16.3	36.6	17.5	21.0	22.1	19.4	24.5	31.8	16.3	13.0	35.1	19.7	37.0	32.0	16.4
D	21.7	22.4	53.1	66.5	12.8	18.0	24.6	14.7	24.7	24.7	23.2	15.8	73.0	10.6	34.3	51.8	29.9
E	32.5	10.6	22.6	60.8	919	19.6	49.6	12.2	32.3	40.1	57.9	10.4	8.7	16.9	36.8	24.2	22.5
F	33.0	23.3	43.9	29.8	15.5	19.6	32.8	43.2	33.2	28.0	31.3	6.0	15.3	27.7	30.0	41.7	9.9
G	39.4	32.1	63.8	32.0	58.4	12.0	17.3	11.2	16.5	23.2	23.7	565	15.3	10.7	32.1	15.6	17.9
H	34.9	38.6	22.1	61.7	17.8	22.3	9.2	11.7	19.7	8.3	58.0	311	1405	45.6	36.2	16.7	111
I	38.3	26.4	48.9	39.4	29.6	31.1	26.5	42.5	32.7	23.6	24.3	72.6	19.5	22.1	71.4	38.2	55.8
J	48.9	38.3	87.8	22.9	26.2	28.9	21.7	18.0	14.6	31.5	16.8	40.5	10.9	11.1	22.2	30.0	12.4
K	62.9	45.2	52.6	39.5	39.3	50.0	21.4	13.4	48.3	46.0	32.9	26.4	68.5	66.9	40.8	16.3	22.4
L	16.6	11.1	37.4	51.0	43.2	44.8	39.8	29.7	74.4	221	38.6	36.6	42.0	58.7	29.7	23.0	21.2
M	21.1	27.5	43.7	26.0	23.5	11.3	20.2	42.7	34.6	33.7	8.0	25.6	25.3	37.8	34.4	11.1	9.6
N	8.5	19.2	26.3	21.2	28.6	14.5	70.2	31.1	48.8	39.2	37.1	31.0	32.6	30.5	21.6	6.7	13.8
O	16.1	28.0	33.7	8.1	15.1	43.5	16.9	23.7	21.0	20.6	19.5	57.1	30.7	23.4	17.9	12.9	15.3
P	19.1	30.0	40.1	41.6	17.7	45.5	20.7	33.5	18.0	20.5	22.8	52.7	39.5	19.0	16.5	10.8	11.9

Table 3. Chemical composition of well discharge sample

(a) Chemical composition of steam condensed water.

Component	Unit	PR-1	PR-8
Electrical conductivity	μS/cm	2360	3180
pH	---	4.90	6.00
Cl	mg/l	0.06	667
NH_4	mg/l	19.7	39.3
As	mg/l	0.03	6.08
Hg	ng/l	5.4	5.7

(b) Gas composition of steam.

		PR-1	PR-8
Liquid-vapor separate pressure		4.8 Kg/cm²G	7.7 Kg/cm²G
Total gas in steam (vol%)		2.20	3.46
Gas composition	H_2S (vol%)	0.7	0.1
	CO_2 (vol%)	98.6	98.9
	H_2 (ppm)	1860	3310
	N_2 (ppm)	1740	2160
	CH_4 (ppm)	3360	4480
	He (ppm)	11.9	14.9
	Ar (ppm)	25.2	29.5

(c) Chemical composition of hot water.

Component	Unit	PR-1	PR-8
Electrical conductivity	μS/cm	4060	4340
Total dissolved solids	mg/l	3830	3670
pH	---	7.80	8.60
Cl	mg/l	1160	929
SO_4	mg/l	44.4	109
H_2CO_3	mg/l	2.7	1.4
HCO_3^-	mg/l	71.2	227
CO_3^{2-}	mg/l	0.3	6.9
Na	mg/l	751	834
K	mg/l	173	136
Ca	mg/l	2.07	1.07
Mg	mg/l	0.35	0.04
Fe	mg/l	0.96	0.06
Al	mg/l	1.25	0.08
SiO_2	mg/l	1090	927
Li	mg/l	6.52	6.40
B	mg/l	174	125
F	mg/l	8.4	7.9
NH_4	mg/l	3.3	2.8
As	mg/l	14.8	12.6
Hg	ng/l	0.23	0.23
D / H	‰(SMOW)	-49.6	-57.0
^{18}O / ^{16}O	‰(SMOW)	+0.7	-1.6
Tritium	T.U.	<0.23	<0.21

Table 4. Chemical geothermometer

well	Geothermometer (°C) Quartz-maximun steam loss	Na/K (Fournier)	Na/K (Truesdell)	Na-K-Ca
PR-1	> 288	301	299	297
PR-8	> 274	263	247	280

II-3 Gravimetric survey

A La Coste & Romberg type gravimeter (G-type) was used for gravimetric survey. Elevation was decided from levellings and measurements by Paulin's precision altimeter.

(1) Measurement and data processing

A gravimetric survey was carried out within Sierra La Primavera Area (238 km²) and within a broader area (14,000 km²) including the above area. 306 points for the Primavera area and 156 points for the broader area were selected out for the survey. Fig. 17 and 22 show the locations of the points.

The value 977,927.15 mgal at the international gravity base point No.04669E in the Meteorological Agency, Mexico City, was adopted as base value. The value 978,188.034 mgal was then determined at the base point (No. 1000) which was set up in Guadalajara Office of C.F.E. for the survey work. To check the in-day change in the gravity, measurements of the gravity were carried out every 30 minutes on 27. August from 6:00 am to 24:00 in Rio Caliente to the West of the area. As a result of that, the gravity values fluctuate between -165 and +85 mgal. On the basis of a curve matching with the theoretical curve, 1.15 was determined as the tidal correction constant. Of 306 points in Sierra La Pimavera area, levellings were made at 291 points. Other points were used for elevation measurement by Paulin's precision altimeter.

The data processing began with the mgal-conversion which converts the read-out values of the gravimeter dial to the gravity unit. Subsequently, the gravity values were calculated

for every measuring point by various corrections such as altitude correction (correction for instrument altitude) caused by difference between measuring and levelling points, tidal correction, drift correction, latitude correction, free-air reduction, Bouguer correction and the topographical correction. The topographical correction of Sierra La Primavera has been carried out based on a site sketch cross section map (up to 20m radius) and on the altitude read out on the topographical map, 20m-60km, and that of the measuring points for the broad area survey has been carried out based on the altitude read out by using 2 charts on a area ranging from the measuring point to 36km.

(2) Feature of Bouguer anomaly distribution in Sierra La Primavera Area

The density of rock samples which were taken in and around the investigation area has been measured to determine the corrected density. Table 5 shows the results divided into geological groups. The table contains 47 samples among which 12 samples are cores. As shown in the Table, the density becomes higher as the rock is older and a remarkable density boundary is observed between tuff and andesite in Cordilleran Volcanics. The average density of the Quaternary which forms the topography of the area is 2.12g/cm^3 according to Table 5. Because of lower density of the Lake Deposites, the corrected density ρ = 2.00g/cm^3 was selected out for a drawing used as Bouguer anomaly map (Fig. 18).

According to Fig. 18, Bougner anomaly values in the area range from - 109 mgal to 126 mgal. The maximum value is located

in the N.W. end, while the minimum value is located near the point No. 112 at the center. Low gravity area with less than -120 mgal occupies a wide range including the middle of the area as center. From a large view point, a big scale low gravity anomaly is observed to be shaped circularly or elliptically with the center located in the middle of the area. The contours are crowded and the Bouguer anomaly values show a remarkable variation at the northern, western and southern ends of these low gravity anomalies. In contrast, the Bougner values variation is less severe at the eastern end. The Bouguer anomaly in the area shows, as described above, a low gravity anomaly as a whole. However, some high gravity anomaly was observed locally. The inside of the low gravity anomaly has a fairly complicated structure. To remove this local anomaly, 2nd and 3rd order trend surface analysis was made against Fig. 18. A trend surface and a residual surface were prepared. Fig. 19 and 20 show the results of 3rd-order analysis. Fig. 19 indicates that the center of Caldera is locate in the vicinity of points No. 87, 89 and 121, and the north and west the north rim of the Caldera has clear borders.

(3) Two dimentional gravity analysis of the cross section

A two-dimentional analysis was carried out in the cross section A-A', B-B' and C-C' in Fig. 18 to investigate the cause of local high gravity anomalies. The results are shown in Fig. 21. The calculation was made based on the Talwani's equation. The 3 layers-structure for the density was assumed in the analysis, defining the 1st layer (ρ = 2-20g/cm^3) consisting of Rhyolite,

Tala Tuff and the Upper Cordilleran Volcanics, the 2nd layer (ρ = 2.40 g/cm^3) of andesite of lower Cordilleran Volcanics, and the 3rd layer (ρ=2.70g/cm^3) as "basement rocks". Further, Lake Deposites (ρ=1.60g/cm^3), Rhyolite (ρ=2.00g/cm^3) and Tala Tuff (ρ=2.00g/cm^3) were partially added to the 1st layer as local low density part. Control points were settled in PR-2 for line A-A', in PR-9 for line B-B' and in PR-5 for line C-C' respectively. Because the upper surface of 3rd layer was confirmed only in PR-9, the surface were regarded as to have equal depth in three profiles. The results include a step-like structure (real line) and a fairly smooth structure (broken line). These 2 structures indicate nearly equal gravity anomalies.

As shown in Fig. 21, the measured anomaly corresponds to the throw provided that it amounts 500-600m. This value is in general conformed with the collapse-throw which was determined by geological survey and well data. The local high gravity anomaly at the center (by Cerritos Colorados) can be interpreted by 400m upheaval of the high density layer. Since elevation by resurgence amounts 260m according to MAHOOD (1980), the high gravity anomaly at the center seems to be caused by the Caldera resurgence. The shape of the resurgence would be rectangular or elliptical with ENE-WSW long axis, as Fig. 18 shows.

Subsequently, a consideration on the local low gravity anomaly is as follows:

By correspondence of Fig. 18 and 21 with the geological map, the gravity anomalies along No. 39. No. 63 and No. 112 are conformed with the Lake Deposites, area with elevated topography.

The fact suggests that it occurred in form of over-correction because of low density (ρ =1.60 g/cm^3) in the formations which produce the heights compared with the corrected density (ρ = 2.00g/cm^3). The above described low gravity anomaly might, therefore, correspond to the thick Lake Deposites area. However, the anomaly by No. 286 corresponds to a area where the Lake Deposits is not distributed showing a low topography. The origin of the anomaly is not clear, but according to an assumption that the section analysis would be successful provided that ρ=2.00g/cm^3 in Fig. 21, it might be attributed to the thick Tala Tuff corresponding to ρ = 2.00g/cm^3.

A structural analizing shown in Fig. 22 can be obtained by summaring the above interpretations. In the drawing, the south rim of Caldera walls is characteristically located in more southern position including the broader area, compared with a conventional geological map. The resurgent and its orientation were clarified by a gravimetric survey, offering useful informations for geothermal surveys as a result.

(4) Characteristics of the regional Bouguer anomaly distribtion

It is difficult to make relationship of the gravity anomaly with the geology in the Sierra La Primavera, being widely covered by the Quaternary. Consequently, the gravimetric survey has been extended as far as the region containing "basement rocks" and the Tertiary, followed by a study on the validity of correspondence of the anomaly which was applied for 2 dimentional with the geology. Fig. 23 shows a regional Bonguer anomaly map with corrected density ρ = 2.20g/cm^3. According to

the Fig. 23, higher Bouguer anomalies (more than -110 mgal) are distributed in the region ranging from SW to W and extending partially to Lake La Vega starting from the north of Ameca.

Based on the geology map (1:100,000) prepared by C.F.E., it can be found the Cretaceous sedimentary rocks and granitic rocks which is the oldest in the area are consistent with the high gravity anomaly. The Paleogene and the Miocene (all consisting of igneous rocks) are also conformed with the local high gravity anomaly. The Pliocene and the Quaternary correspond in general to the low gravity anomaly, except for Tequila Volcano and Cerro Grande to the east.

The above results are harmonized with the density dividing shown in Table 5 and with the layer dividing estimated by the 2 dimentional-analysis. Furthermore, the orientations of NW-SE and N-S trend can be read out from the shape of the gravity anomaly. These are coincided with those of Tepic-Chapala structural trend (NW-SE) and Colima structural trend (N-S) respectively clarified by a geological survey.

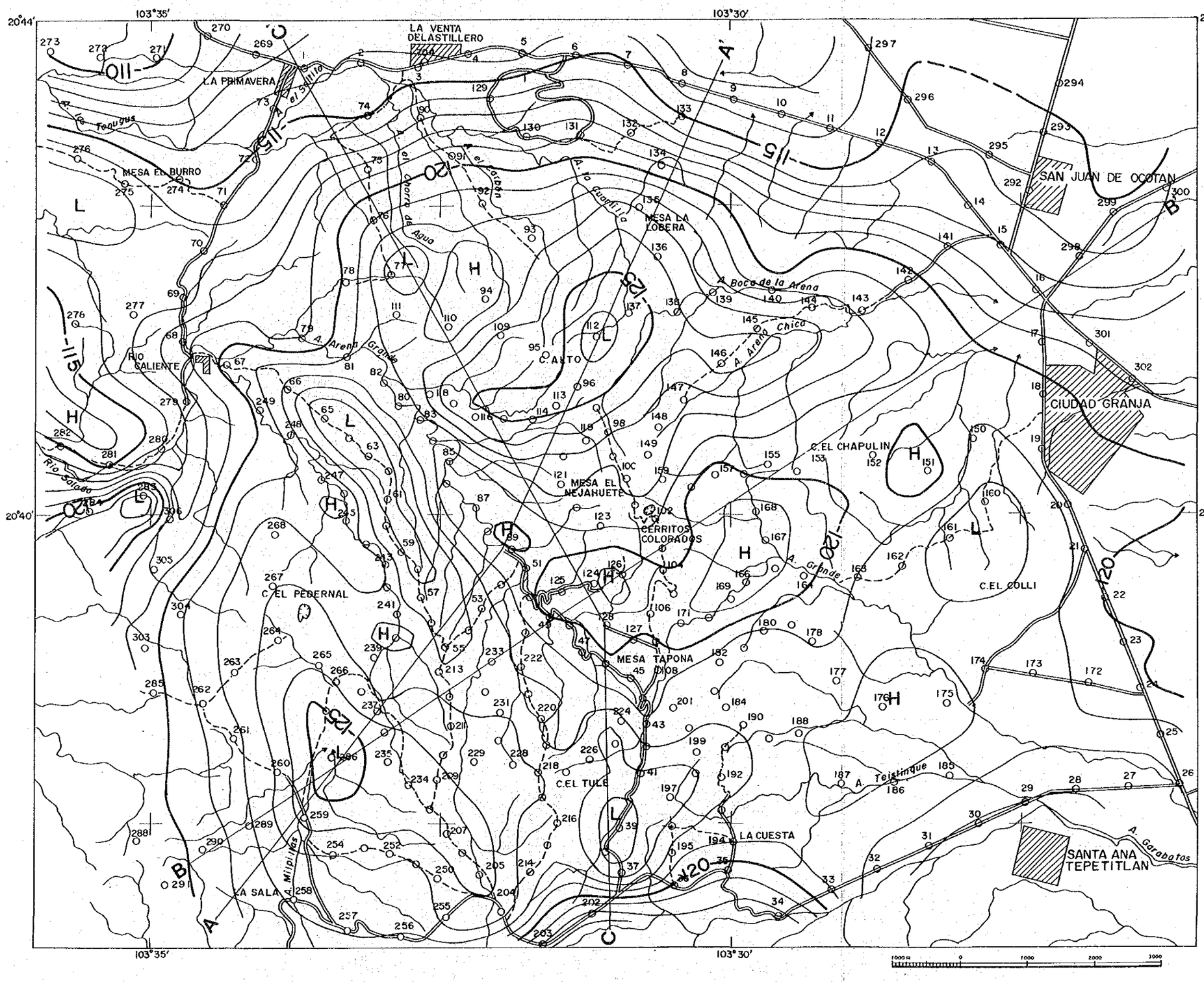

Fig. 18. Bouguer anomaly map $\rho = 2.00 g/cm^3$

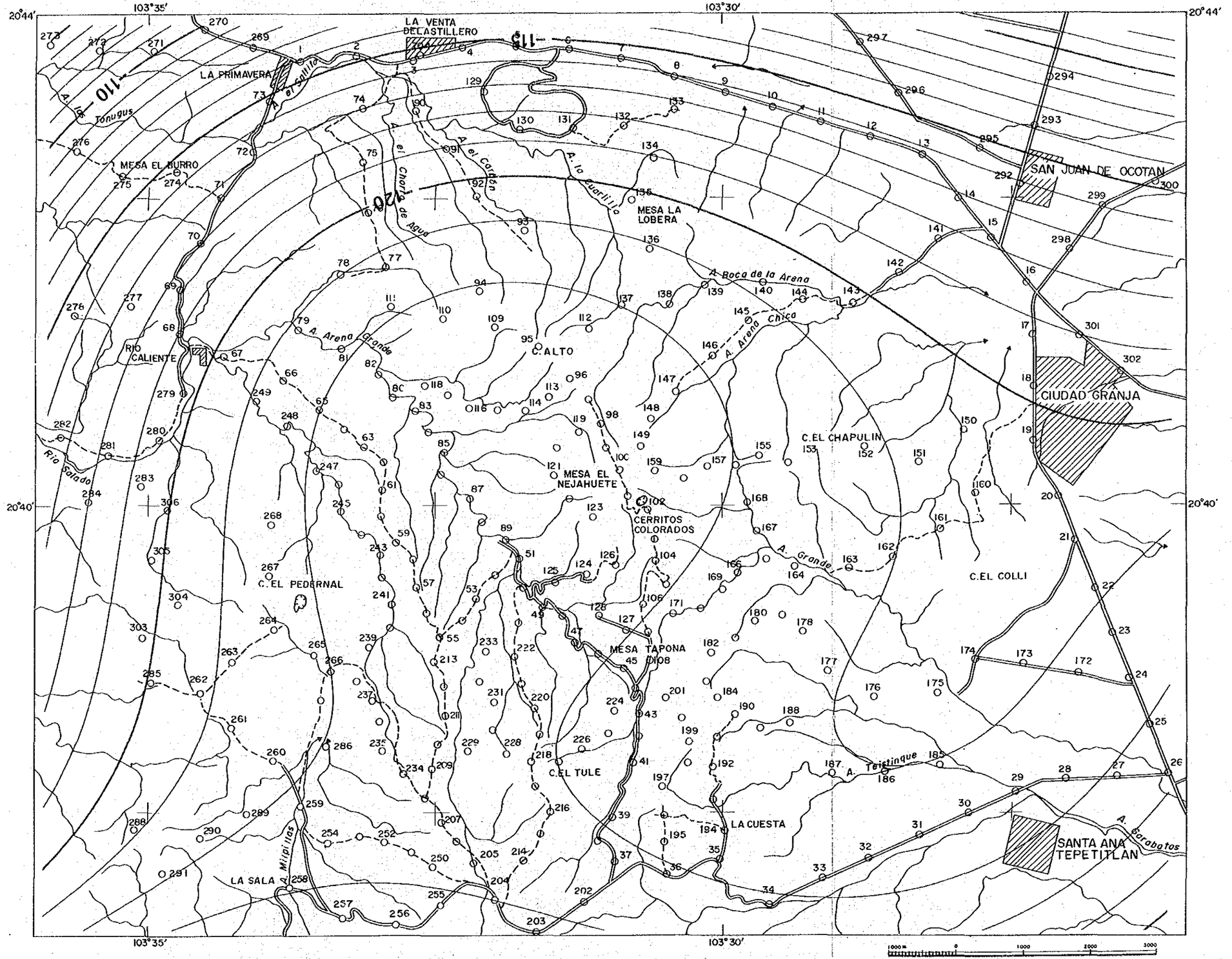

Fig. 19. Third-order trend surface

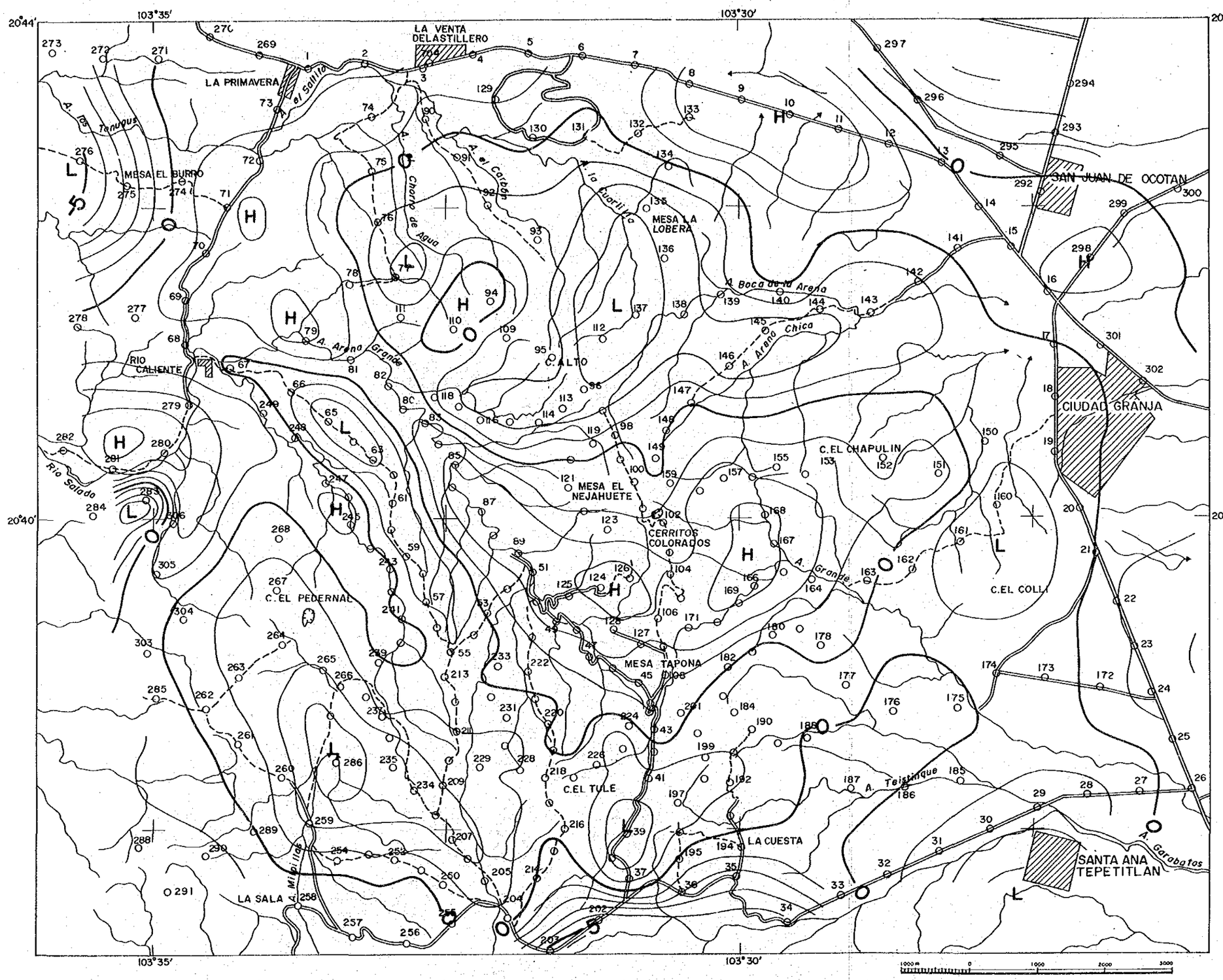

Fig. 20. Residual of third-order trend surface

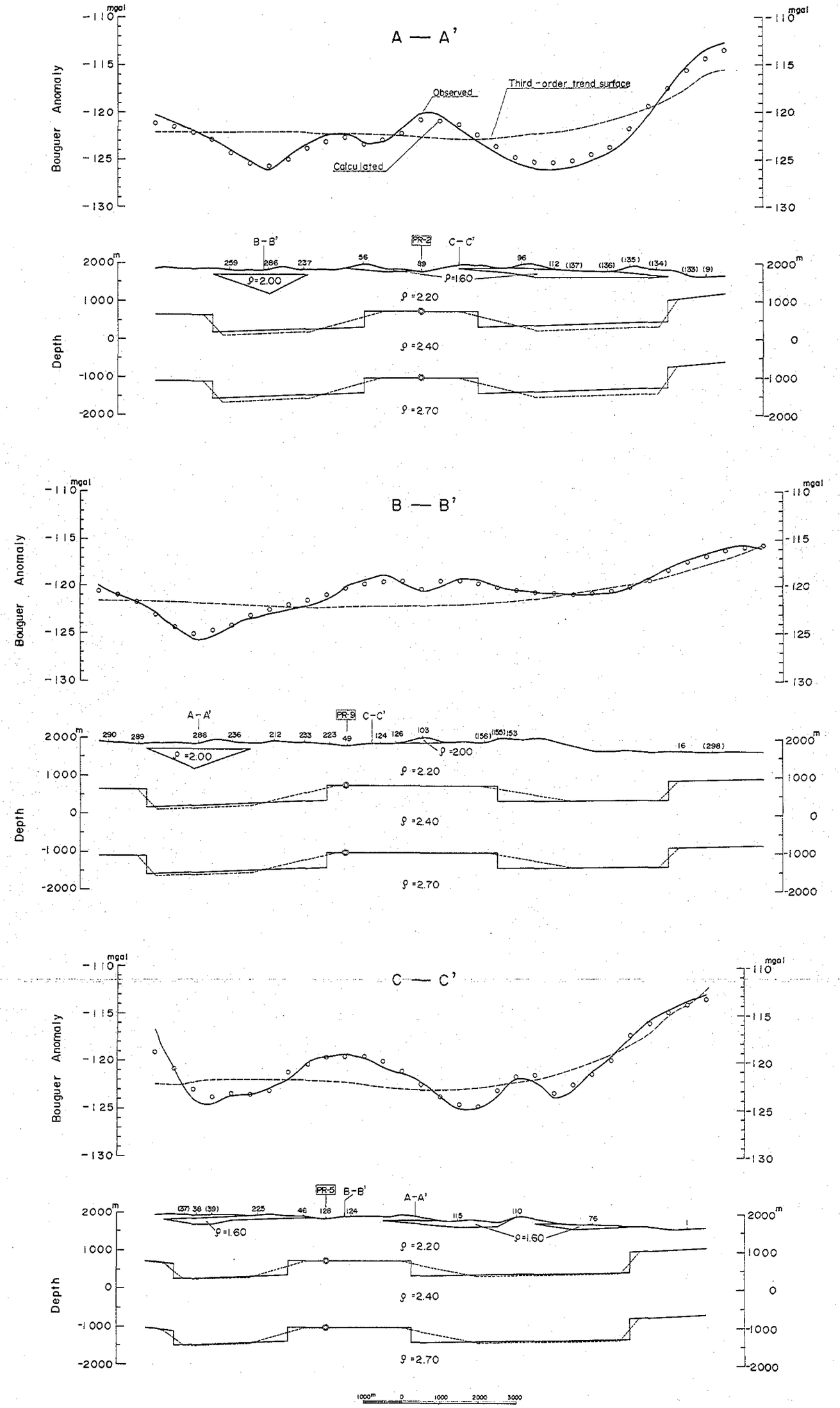

Fig. 21. 2-dimentional gravity analysis, lines A-A' B-B' and C-C' show in Fig. 17

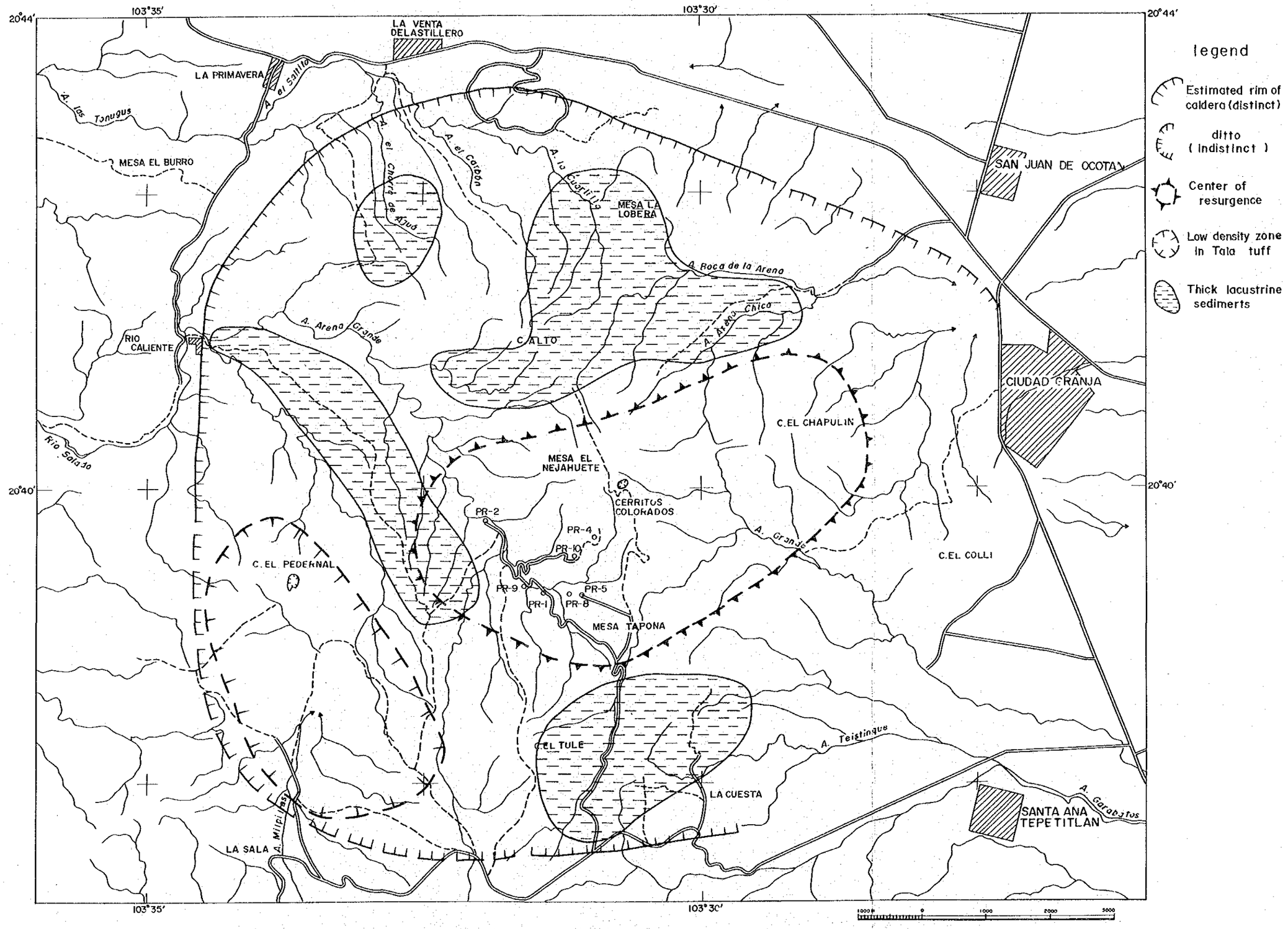

Fig. 22. Structural analizing map of gravity survey

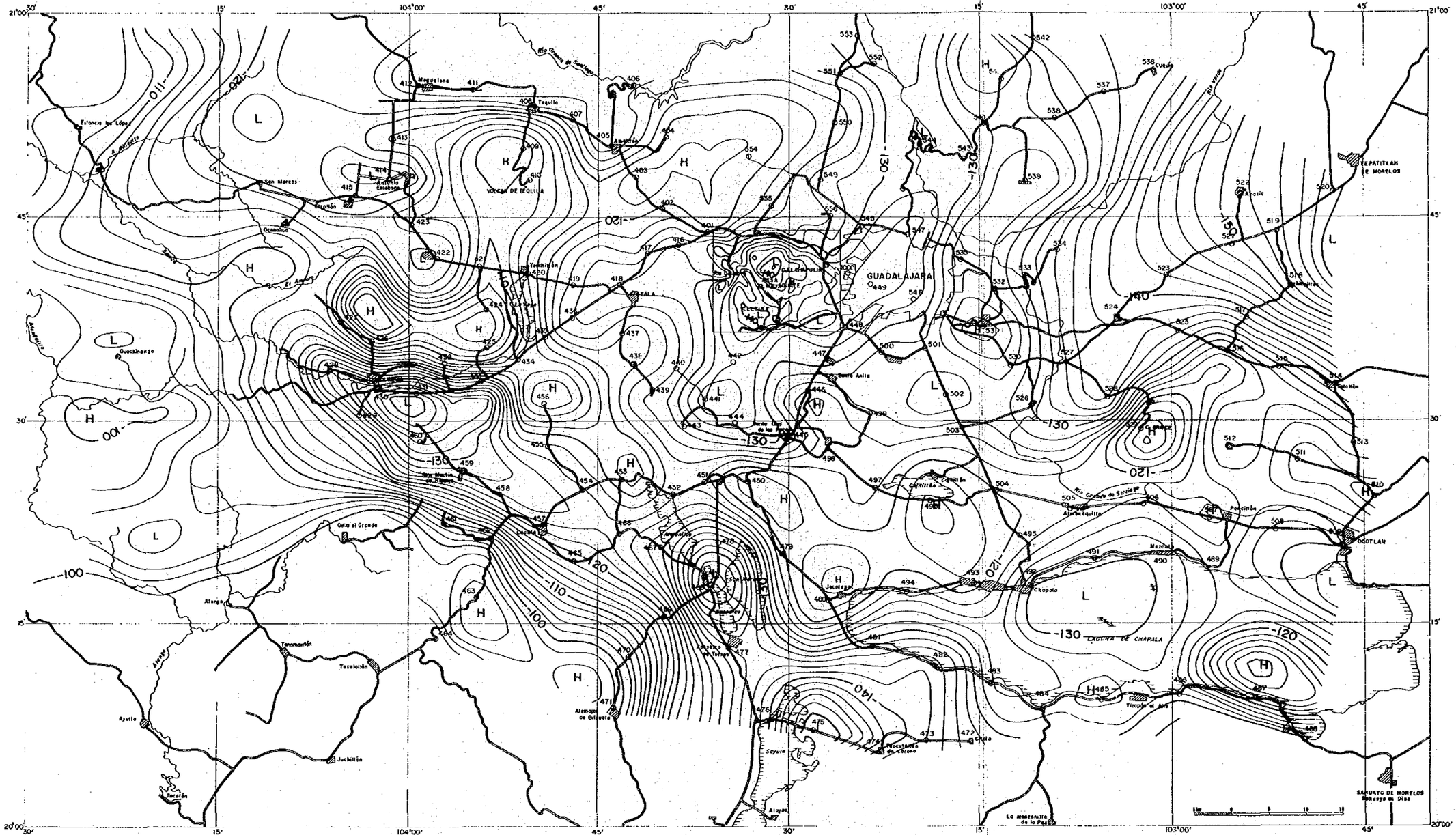

Fig. 23. Regional Bouguer anomaly map $\rho = 2.20 g/cm^3$

Table 5. Densities of rock samples

Geology		Wet Density (g/cm³) 2.0 2.5	Number of Sample	Mean Density(g/cm³)		
Quaternary	rhyolite (Central Dome)	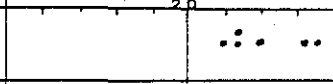	6	2.21	2.12	2.21
	Welded tuff (Tala tuff)	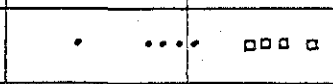	9	2.06		
Tertiary	rhyolite	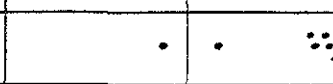	10	2.33	2.28	
	tuff	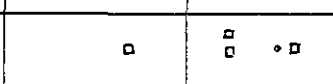	7	2.22		
	andesite		7	2.39		
	basalt		6	2.60		
Cretaceous sedimentary rock		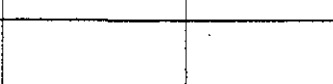	2	2.57		

• Surface Sample ▫ core Sample

II-4 Electrical survey (MT method)

The Remote Reference Magnetotelluric method was carried out as electrical survey in this area. The sounding points were arranged with interval of about 300m in and around the geothermal wells and of about 500m in other area. Measurements in the area of steep Sopography were made by remove of equipments according to topographical situation.

(1) measurement and data processing

54 sounding station were selected around the geothermal manifestation area (Fig. 24) to implement the Remote Reference Magnetotelluric Method. Among 54 points 8 were tried resounding to verify the data quality and get fair data files as possible. Table 6 shows recording band width, parameters and duration. Fig. 25 shows the data acquisition system. Becasue the field processor was able to process data in real time while acquiring, apparent resistivity curves (Fig. 26), phase curves etc.could be calculated and displayed on the field. For the purpose of data improvement by quality control of the data, both the Remote Reference (simultaneous measuring at 2 points). Processing and the Single Data Processing have been implemented on each point.

During final data processing, correlation of the electric field with the magnetic field (coherency check) was check, and after removing automatically ranges of low data quality, FFT (First Fouries Transform) processing was made to calculate and indicate the following parameters:

(1) apparent resistivity (ρxy, ρyx)

(2) phase (ϕxy, ϕyx)

(3) impedance strike

(4) tipper strike

(5) tipper magnitude

(6) skew

(2) model inversion analysis and structure index

At first, to calculate the underground apparent resistivity, an one-dimentional model inversion analysis was carried out under the assumption of horizontal multilayer structure in underground. Fig. 27 shows the analysis procedure. As shown in Fig. 27, the important point of the analysis is to put the resistivity of and the thickness the horizontal multi-layer into the apparent resistivity-frequency curves by various value assumption for obtaining an adequate resistivity value. Fig. 28 shows an example of the inversion analysis.

For such model inversion analysis, there is a problem of adaptability when the subsurface has no horizontal multi-layer strucsture. If, for example the structure is 2 or 3 dimensional, how could be adopted the 1 demensional analysis? In case of 2 dimensional resistivity of subsurface, 2 mode types can be generally considered based on the apparent resistivities ρxy, ρyx obtained:

TE mode: direction of the electric field is parallel to the structure axis.

TM mode: direction of the magnetic field is parallel to the structure axis.

The magnetic field changes easily depending on surrounding geological situations (rock magnetism, alteration etc.) and on

the lateral influence. So, it is not suitable for 1 dimensional analysis. Accordingly, TE mode was selected out for the present analysis.

For determining TE mode out of ρxy and ρyx, angles of the tipper strike (indicating the TE direction) and of the impedance strike (indicating the xy direction) were checked. If the angle is smaller than $\pi/4$, $\rho x y$ is TE mode. If the angle is bigger than $\pi/4$, ρyx becomes TE mode.

Tipper magnitude (T) and skew (S) were used to judge the dimension of underground resistivity structure:

1 dimentional structure: $T \fallingdotseq 0$ and $S \fallingdotseq 0$

2 dimentional structure: $T \gg 0$ and $S \fallingdotseq 0$

3 dimentional structure: $T \gg 0$ and $S \gg 0$

Fig. 29 and 30 show distribution drawings for tipper magnitude and skew respectively. This area shows as a whole the 1 dimensional structure except for some 2 dimensional structures by points 01 and 46. No 3 dimensional structure was observed in this area.

(3) horizontal profile analysis

Apparent resistivity distribution drawings with TE mode were prepared on 3 periods (0.01s, 1s, 30s) to determine apparent resistivity in the horizontal profile. Fig. 31 shows a distribution drawing on 30s period base. As shown in Fig. 31, there is a low apparent resistivity zone to the South of PR-1 and PR-8 in a deep subsurface of this area. NW-SE trend of the zone could be found.

Then, applying the Bostic inversion to the initial apparent

resistivity-period curve, a resistivity-depth curve was drawn. A horizontal-profile was prepared on TE mode by extracting resistivity value on each sounding point at optional depth. 6 levels with 500m interval from 1,500m to -1,000m(above sea level) together with a -3,000m level, totally 7 depth levels were selected for preparing horizontal profiles. Among them, Fig. 32-33 show horizontal profile of 0m and-500m altitude (1,800 and 2,300m depth) which is considered as a main reservior in this area. According to the Figures, low resistivity zones with less than 5 m are localized in the South of PR-8, PR-2 and in the south of the area. In addition, the low resistivity zone in the south of PR-8 occurs also on the -3,000m horizontal plan and is conformed with both uplift zone found by geological survey and upflow zone found by well temperature and fluid inclusion measurement. This is worthy of attention.

(4) vertical profile analysis

Survey line B (section E-W) and 3 (section S-N) were used for preparing apparent resistivity-period drawing to know the apparent resistivity in vertical profile (see Fig. 34 for line 3 profile). For position of the survey line, refer to Fig. 24.

In case of line B, high apparent resistivity zones with more than 50m are nearly continuously distributed at the short period range, while both high and low apparent resistivity zones occur alternately at the long period range.

In case of line 3, on the other hand, a low apparent resistivity zone occurs enclosing the sounding point 18, and it shows an expanding shape from the deep bottom to the top and

side.

Subsequently, similar to the horizontal profile analysis, a resistivity-depth section drawing was prepared after Bostic inversion. The resistivity pattern for line B is fairly same as that of the above mentioned apparent resistivity, while the pattern for line 3 is different from that of Fig. 34. The low resistivity zone enclosing Point 18 is distributed vertically and continuously from deep to shallow position and seems to suggest an existence of upflow in this region (Fig. 35).

A 1-dimentional model profile can be made by connecting the values of resistivity and layer thickness obtained from inversion each other along the survey line. Profile were prepared for 9 survey lines of which line B and 3 as a representation have been used to make model profile shown in Fig. 36 and 37. The Figures show a typical 3 layer structure consisting of high resistivity layer in the shallow part low resistivity layer in the middle part and of high resistivity layer in the deep part. The first layer seems to reflect a dry Tala Tuff Formation. This is harmonized with the fact that the geothermal fluid flashes in the formation according to the well tests of PR-1 and PR-8 (i.e. water shortage in shallow formation). Low resistivity values in the middle are homogeneous for Line 3, while divergent for Line B depending on the position on the line. By plotting tracks of existing wells into Fig 36, it was found that drillings have attained to the low resistivity zone in case of wellbore offering large steam production.

Therefore, an attention should be paid to this low re-

sistivity zone in the middle as prospective geothermal reservior with dominating fractures. There is a low resistivity occurence at point 18 in the deep showing a totally different type from neighborhoods. It appears to have corelation with the upflow. A 2-dimentional model analysis also have been carried out for line B and 3. The result of this analysis shows the same resistivity distribution and structure as 1-dimensional profile, and emphasized the horizontal multilayer structure. For instance, it is characteristic that resistivies are lower at the basal part of line B and point 18 (Fig. 38 and 39).

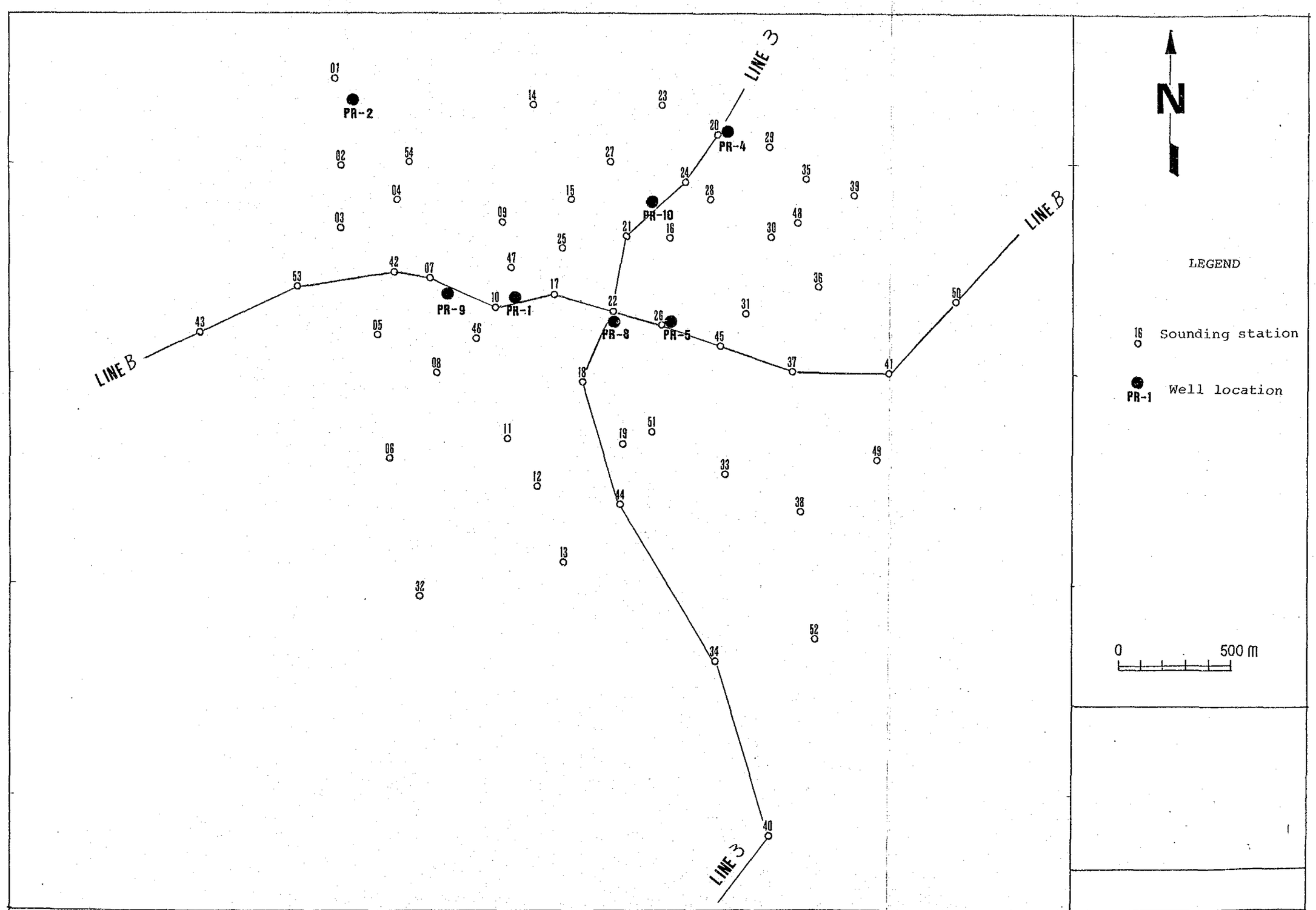

Fig. 24. Location and line map of MT survey

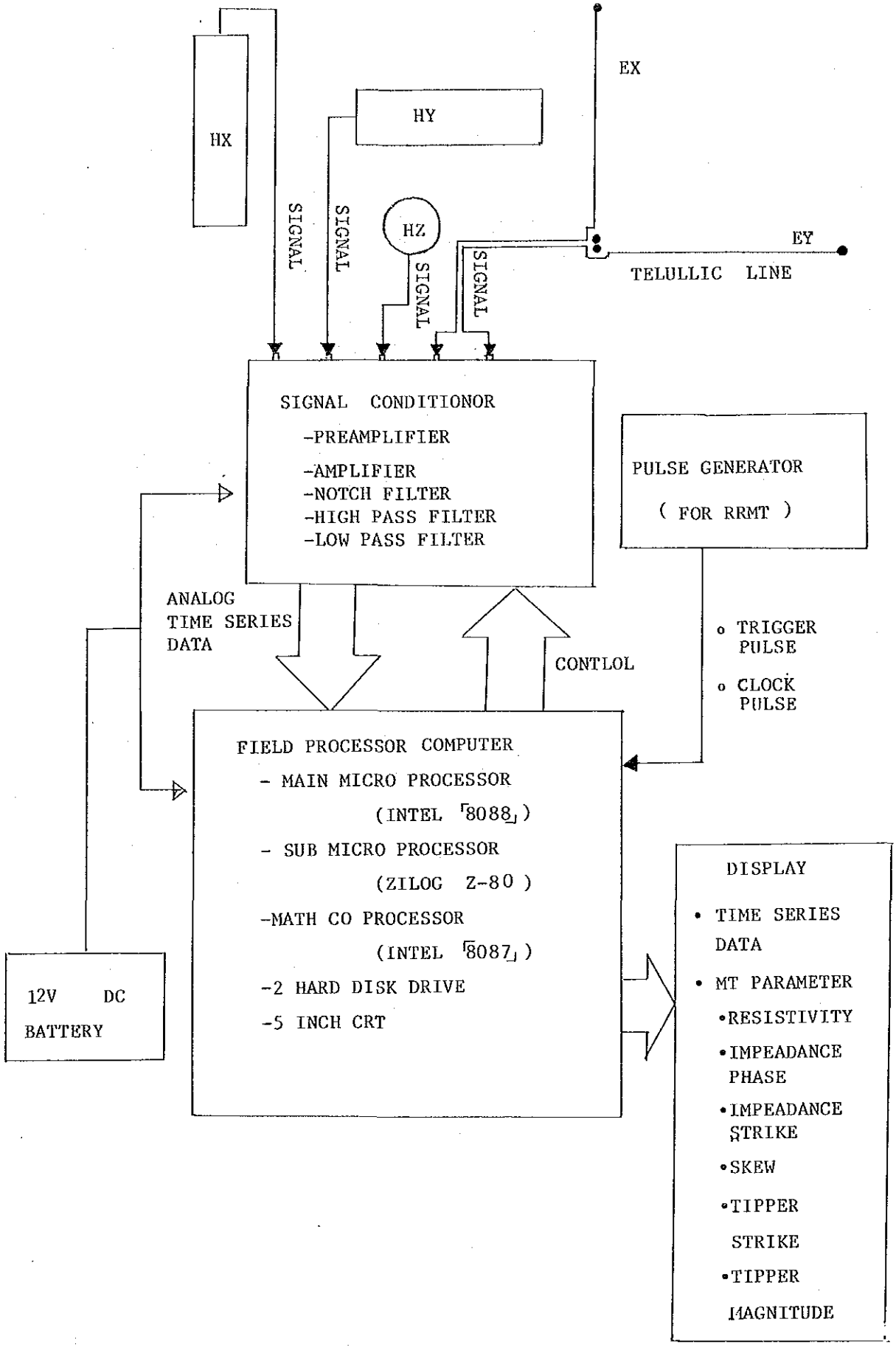

Fig. 25. Outline of MT data acquisition system

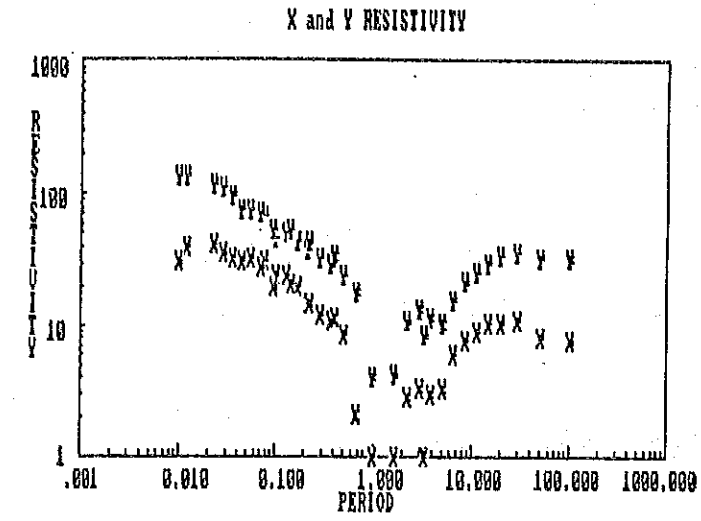

a) Single Data Processing Result using Field Processor (in Field)

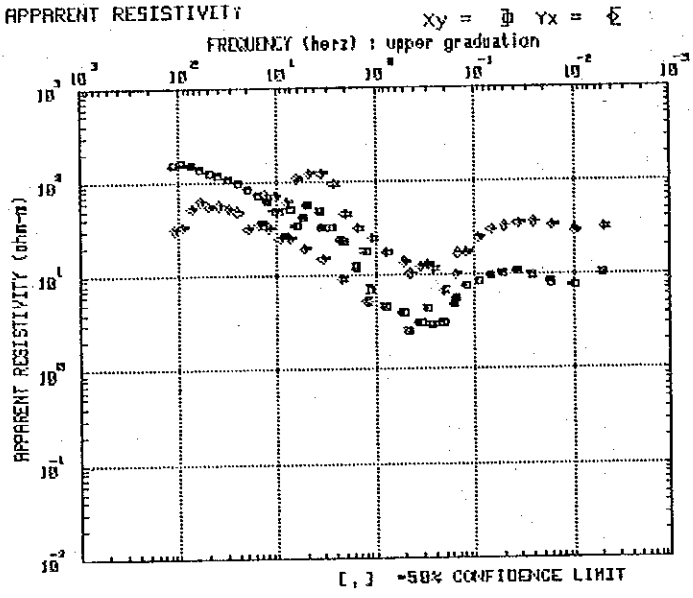

b) Single Data Processing Result after editting using Data Processing System

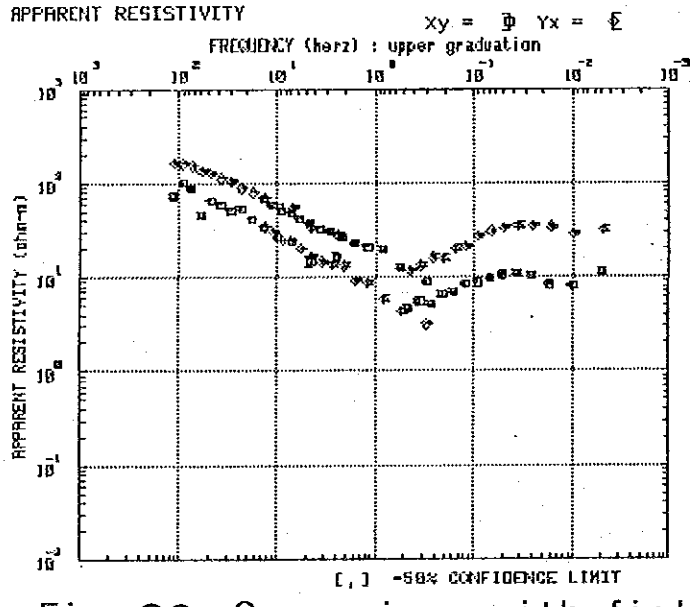

c) Final Remote Reference Data Processing Result using Data Processing System

Fig. 26. Comparison with field processor and final data processing, station 07

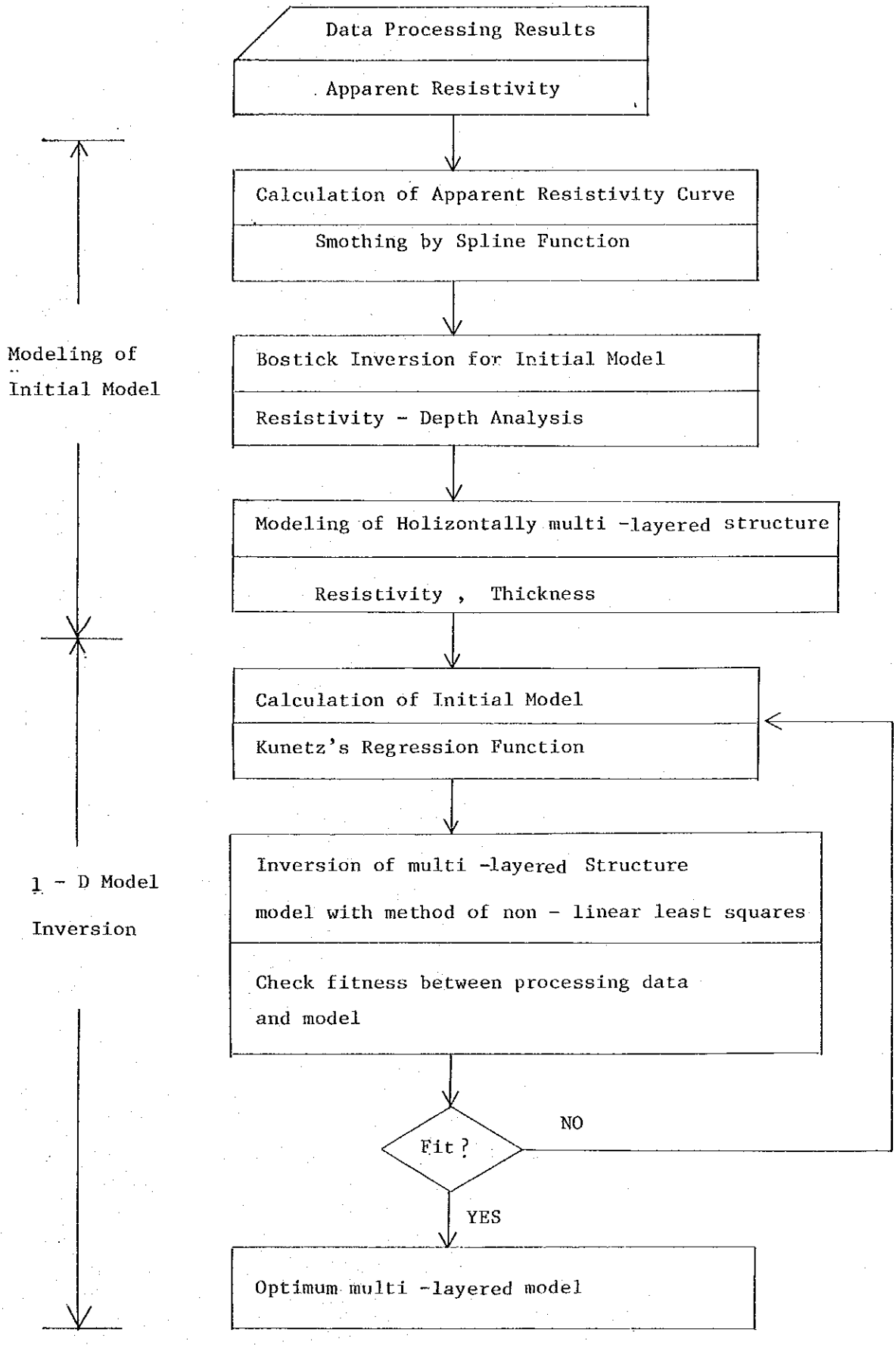

Fig. 27. Flowchart of 1-D model inversion

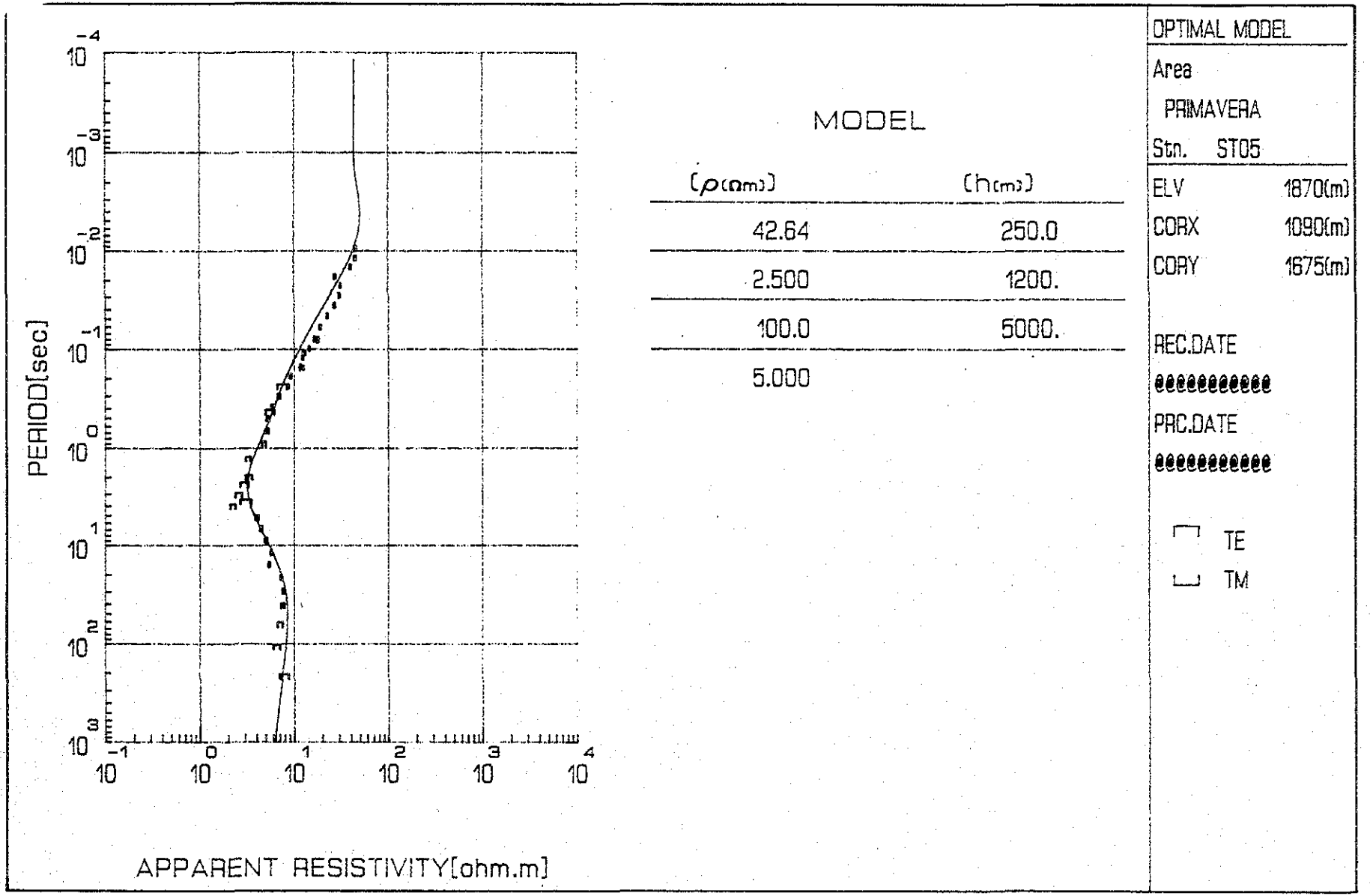

Fig. 28. Example of 1-D model inversion result, station 05